

1 **Parameter regionalization of a monthly water balance model for**
2 **the conterminous United States**

3 **Andrew R. Bock¹, Lauren E. Hay², Gregory J. McCabe², Steven L. Markstrom², and R.**
4 **Dwight Atkinson³**

5 ¹ U.S. Geological Survey, Colorado Water Science Center, Denver Federal Center, P.O. Box
6 25046, MS 415, Denver, Colorado, 80225, USA

7 ² U.S. Geological Survey, National Research Program, Denver Federal Center, P.O. Box 25046,
8 MS 413, Denver, Colorado, 80225, USA

9 ³ U.S. Environmental Protection Agency, Office of Water (4503-T), 1200 Pennsylvania Ave.,
10 Washington, DC, 20004, USA

11
12 Correspondence to: A. Bock (abock@usgs.gov)

26 **Abstract**

27 A parameter regionalization scheme to transfer parameter values from gaged to ungaged areas
28 for a monthly water balance model (MWBM) was developed and tested for the conterminous
29 United States (CONUS). The Fourier Amplitude Sensitivity Test, a global-sensitivity algorithm,
30 was implemented on a MWBM to generate parameter sensitivities on a set of 109,951 hydrologic
31 response units (HRUs) across the CONUS. The HRUs were grouped into 110 calibration
32 regions based on similar parameter sensitivities. Subsequently, measured runoff from 1,575
33 streamgages within the calibration regions were used to calibrate the MWBM parameters to
34 produce parameter sets for each calibration region. Measured and simulated runoff at the 1,575
35 streamgages showed good correspondence for the majority of the CONUS, with a median
36 computed Nash-Sutcliffe Efficiency coefficient of 0.76 over all streamgages. These methods
37 maximize the use of available runoff information, resulting in a calibrated CONUS-wide
38 application of the MWBM suitable for providing estimates of water availability at the HRU
39 resolution for both gaged and ungaged areas of the CONUS.

40

41

42

43

44

45

46

47

48

49 **1 Introduction**

50 The WaterSMART program (<http://water.usgs.gov/watercensus/WaterSMART.html>) was started
51 by the United States (U.S.) Department of the Interior in February 2010. Under WaterSMART,
52 the National Water Census (NWC) was proposed as one of the U.S. Geological Survey's (USGS)
53 key research directions with a focus on developing new hydrologic tools and assessments. One
54 of the major components of the NWC is to provide estimates of water availability at a sub-
55 watershed resolution nationally (<http://water.usgs.gov/watercensus/streamflow.html>) with the
56 goal of determining if (1) the Nation has enough freshwater to meet both human and ecological
57 needs and (2) this water will be available to meet future needs. Streamflow measurements do not
58 provide direct observations of water availability at every location of interest; approximately 72
59 percent (%) of land within the conterminous U.S. is gaged, with approximately 13% of these
60 gaged areas being unaffected by anthropogenic effects (Kiang et al., 2013). This creates the
61 challenge of determining the best method to transfer information from gaged catchments to data-
62 poor areas where results cannot be calibrated or evaluated with measured streamflow (Vogel,
63 2006). This transfer of model parameter information from gaged to ungaged catchments is
64 known as hydrologic regionalization (Blöschl and Sivapalan, 1995).

65 Many hydrologic regionalization methods have focused on developing measures of similarity
66 between gaged and ungaged catchments using spatial proximity and physical characteristics.
67 These methods are highly dependent on the complexity of the terrain and scale at which the
68 relations are derived. Spatial proximity is considered the primary explanatory variable for
69 hydrologic similarity (Sawicz et al., 2011) because of the first-order effects of climatic and
70 topographic controls on hydrologic response. Close proximity, however, does not always result
71 in hydrologic similarity (Vandewiele and Elias, 1995; Smakhtin, 2001; Ali et al., 2012).

72 Physical characteristics have been used as exploratory variables to develop a better
73 understanding of the relation between model parameters that represent model function, and
74 physical properties of the catchment (Merz and Blöschl, 2004). The relation between model
75 parameters and the relevant physical characteristics, expressed for example as a form of
76 multivariate regression, can be transferred to ungaged catchments (Merz and Blöschl, 2004).
77 Model parameter definitions are by nature ambiguous and often difficult to correlate to a small

78 number of meaningful variables such as physical and climatic characteristics (Zhang et al.,
79 2008); some studies have found no significant correlation between catchment attributes and
80 model parameters (Seibert, 1999; Peel et al., 2000), whereas others found that high correlation
81 does not guarantee parameters that result in reliable model simulations of measured data (Sefton
82 and Howarth, 1998; Kokkonen et al., 2003; Oudin et al., 2010). Physical characteristics also are
83 used to classify catchments into discrete regions or clusters based on similarity in multi-
84 dimensional attribute space (Oudin et al, 2008, 2010; Samuel et al., 2011). While these methods
85 have indicated some success in simulating behavior of specific hydrologic components, such as
86 base flow (Santhi et al., 2008), other efforts utilizing discrete clusters performed poorly in
87 explaining variability of measured streamflow (McManamay et al., 2011).

88 Two important components of the transfer of parameters to ungaged catchments are the
89 identification of (1) influential (and non-influential) parameters, and (2) geographic extents and
90 scales at which parameters exert control on model function. Reducing the number of parameters
91 is important for calibration efficiency by reducing the structural bias of the model and the
92 uncertainty of results where they cannot be verified or confirmed (van Griensven et al., 2006). A
93 high number of calibrated, poorly constrained parameters can often mask data or structural
94 errors, which can go undetected and reduce the skill of the model in replicating results outside of
95 calibration conditions (Kirchner, 2006; Blöschl et al., 2013). This increases the potential for
96 equifinality of parameter sets and higher model uncertainty that can be propagated to model
97 results (Troch et al., 2003).

98 Sensitivity analysis (SA) has advanced the understanding of parameter influence on model
99 behavior and structural uncertainty. SA measures the response of model output to variability in
100 model input and/or model parameter values. SA partitions the total variability in the model
101 response to each individual model parameter (Reusser et al., 2011) and results in a more-defined
102 set of parameters and parameter ranges. Identification of sensitive parameters and their ranges is
103 important for hydrologic model applications as key model parameters can vary spatially across
104 physiographic regions, and also temporally (Tang et al., 2007; Guse et al., 2013).

105 Until recently, the high computational demands of SA have limited most implementations of
106 hydrologic model SA to local sensitivity algorithms that evaluate a single parameter at a time

107 (Tang et al., 2007). Global SA uses random or systematic sampling designs of the entire
108 parameter space to quantify variation in model output (van Griensven et al. 2006, Reusser et al.
109 2011). Some of these methods can account for parameter interaction and quantify sensitivity in
110 non-linear systems. Global SA methods are computationally intensive (Cuo et al., 2011), but
111 ever increasing computational efficiency has allowed for the development and application of a
112 large number of global SA algorithms.

113 Previous work has suggested that isolating the key parameters that control model performance
114 can be used to infer dominant physical processes in the catchment, as well as which components
115 of the model dominate hydrologic response (van Griensven et al. 2006, Tang et al., 2007,
116 Reusser et al., 2011). To date, there has been little analysis of the use of SA for deriving
117 measures of hydrologic similarity across catchments that can be applied towards hydrologic
118 regionalization of model parameters. The spatially-distributed application of SA could be used
119 to provide additional information for the delineation of homogeneous regions for parameter
120 transfer based on similarity of model results from the SA. This strategy allows for the use of the
121 existing model information and configuration to develop a calibration and regionalization
122 framework without significantly changing the model structure or implementation

123 In this study, we present a hydrologic regionalization methodology for the CONUS that derived
124 regions of hydrologic similarity based on the response of a Monthly Water Balance Model
125 (MWBM) to parameter SA. Groups of streamgages within each region are calibrated together to
126 define a single parameter set for each region. By extending model calibration to a large number
127 of sites grouped by similarity through a quantified measure of model behavior, a more specific
128 and constrained parameter space that fits each region can be identified.

129 **2 Methods**

130 **2.1 Monthly Water Balance Model**

131 The MWBM (Fig. 1) is a modular accounting system that provides monthly estimates of
132 components of the hydrologic cycle by using concepts of water supply and demand (Wolock and
133 McCabe 1999; McCabe and Markstrom, 2007). Monthly temperature (T) is used to compute
134 potential evapotranspiration (PET) and to partition monthly precipitation (P) into rain and snow

135 (Fig. 1). Precipitation that occurs as snow is accumulated in a snow pack (snow storage as snow
136 water equivalent, or SWE); rainfall is used to compute direct runoff (R_{direct}) or overland flow,
137 actual evapotranspiration (AET), soil-moisture storage recharge, and surplus water, which
138 eventually becomes runoff (R) (Fig. 1). When rainfall for a month is less than PET, AET is equal
139 to the sum of rainfall, snowmelt, and the amount of moisture that can be removed from the soil.
140 The fraction of soil-moisture storage that can be removed as AET decreases linearly with
141 decreasing soil-moisture storage; that is, water becomes more difficult to remove from the soil as
142 the soil becomes drier and less moisture is available for AET. When rainfall (and snowmelt)
143 exceeds PET in a given month, AET is equal to PET; water in excess of PET replenishes soil-
144 moisture storage. When soil-moisture storage reaches capacity during a given month, the excess
145 water becomes surplus and a fraction of the surplus (R_{surplus}) becomes R, while the remainder of
146 the surplus is temporarily held in storage. The MWBM has been previously used to examine
147 variability in runoff over the CONUS (Wolock and McCabe, 1999; Hay and McCabe 2002;
148 McCabe and Wolock, 2011a) and the global extent (McCabe and Wolock, 2011b). Table 1 lists
149 the MWBM parameters, with definitions and parameter ranges for calibration.

150 The Ppt_{adj} and Tav_{adj} parameters specify seasonal adjustments for precipitation and
151 temperature, respectively. The seasonal adjustment parameters were included to account for
152 errors in the precipitation and temperature data used in this analysis. Sources of systematic and
153 non-systematic errors of climate forcing data are well documented from the precipitation gage-
154 derived sources (Groisman and Legates, 1994; Adam and Lettenmaier, 2003). Interpolation of
155 these systematic errors from point-scale to gridded domains may propagate these biases,
156 especially in complex terrain (Clark and Slater, 2006; Oyster et al, 2015). The use of adjustment
157 factors allows uncertainty associated with forcing data and model parameter values to be treated
158 separately (Vrugt et al., 2008).

159 *Figure 1. Conceptual diagram of the Monthly Water Balance Model (McCabe and Markstrom*
160*Table 1. 2007). Processes influenced by model parameters used in Fourier Amplitude Sensitivity Test*
161 *(FAST) those identified by green arrow and numbered 1-5 (Table 1).*

162 Monthly Water Balance Model parameters and ranges.

163 The MWBM was applied to the CONUS with 109,951 hydrologic response units (HRUs) from
164 the Geospatial Fabric (Viger and Bock, 2014), a national database of hydrologic features for
165 national hydrologic modeling applications (Fig. 2). This HRU derivation is based on an
166 aggregation of the NHDPlus dataset (U.S. Environmental Protection Agency and U.S.
167 Geological Survey, 2010), an integrated suite of geospatial data that incorporates features from
168 the National Hydrography Dataset (<http://nhd.usgs.gov/>), the National Elevation Dataset
169 (<http://ned.usgs.gov/>), and the Watershed Boundary Dataset (<http://nhd.usgs.gov/wbd.html>). The
170 sizes of the HRUs range from less than 1 square kilometer (km²) up to 67,991 km², with an
171 average size of 74 km².

172 Inputs to the MWBM by HRU are: (1) monthly P (millimeters), monthly mean T (degrees
173 Celsius), (2) latitude of the site (decimal degrees), (3) soil moisture storage capacity
174 (millimeters), and (4) monthly coefficients for the computation of PET (dimensionless).
175 Monthly P and mean T were derived from the daily time step, 1/8° gridded meteorological data
176 for the period of record from January 1949 through December 2011 (Maurer et al., 2002).
177 Monthly P and T data were aggregated for each HRU using the USGS Geo Data Portal
178 (<http://cida.usgs.gov/climate/gdp/>) (Blodgett et al., 2011). Latitude was computed from the
179 centroid of each HRU. Soil moisture storage capacity was calculated using a 1 km² grid derived
180 from the Soils Data for the Conterminous United States (STATSGO) (Wolock, 1997). The
181 monthly PET coefficients were calculated by calibrating the Hamon PET values to Farnsworth et
182 al. (1982) mean monthly free-water surface evapotranspiration. McCabe et al. (2015) describes
183 these PET coefficient calculations in detail.

184 *Figure 2. Hydrologic Response Units of the Geospatial Fabric, differentiated by color, overlain*
185 *by NHDPlus region boundaries (R01-R18).*

186 **2.2 Fourier Amplitude Sensitivity Test**

187 A parameter SA for the CONUS was conducted for the MWBM using the Fourier Amplitude
188 Sensitivity Test (FAST) to identify areas of hydrologic similarity. FAST is a variance-based
189 global sensitivity algorithm that estimates the contribution to model output variance explained by
190 each parameter (Cukier et al. 1973, 1975; Saltelli et al. 2000). Advantages of using FAST over

191 other SA methods are that FAST can calculate sensitivities in non-linear systems, and is
192 extremely computationally efficient. The seasonal adjustment factors were not incorporated into
193 the FAST analysis. We viewed the seasonal adjustment factors as more related to the forcing
194 data, and for this application only parameters associated with model structure were included
195 (first five parameters in Table 1).

196 FAST transforms a model's multi-dimensional parameter space into a single dimension of
197 mutually independent sine waves with varying frequencies for each parameter, while using the
198 parameter ranges to define each wave's amplitude (Cukier et al. 1973, 1975; Reusser et al.
199 2011). This methodology creates an ensemble of parameter sets numbering from 1 to N, each of
200 which is unique and non-correlated with the other sets. Parameter sets are derived using the
201 corresponding y-values along each parameter's sine wave given a value on the x-axis. The
202 model is executed for all parameter sets using identical climatic and geographic inputs for each
203 simulation. The resulting series of model outputs are Fourier-transformed to a power spectrum
204 of frequencies for each parameter. Parameter sensitivity is calculated as the sum of the powers
205 of the output variance for each parameter, divided by the sum of the powers of all parameters
206 (Total Variance). The parameter sensitivities are scaled so that the sensitivities for all
207 parameters sum to 1. Thus, parameters that explain a large amount of variability in the model
208 output have higher (i.e. closer to 1) parameter sensitivity values.

209 FAST was implemented with the MWBM using the 'fast' library in the statistical software R
210 (Reusser, 2012; R Core Team, 2013). Parameter ranges used by FAST for generating wave
211 amplitudes of parameter ensembles across the CONUS were based on table 1. The 'fast' R
212 package pre-determines the minimal number of runs necessary to estimate the sensitivities for
213 the given number of parameters (Cukier et al., 1973). For our application we generated an
214 ensemble of 1000 parameter sets (as compared to the minimally suggested number of 71
215 estimated by 'fast'). The use of the minimal number of parameter sets should be a consideration
216 for more complex models, but the relative computational efficiency and parallelization of the
217 MWBM allowed the model to simulate this larger number of parameter sets quickly to help
218 ensure a robust parameter sensitivity analysis.

219 Many applications of SA in hydrologic modeling have evaluated parameter sensitivity for
220 measured streamflow using performance-based measures such as bias, root mean squared error
221 (RMSE), and the Nash-Sutcliffe Efficiency (NSE) (Nash and Sutcliffe, 1970; Moriasi et al.,
222 2007). In this study, parameter sensitivity is examined using two hydroclimatic indices that
223 account for the magnitude and variability of both climatic input and model output: the (1) Runoff
224 Ratio (RR), a ratio of simulated runoff to precipitation, and (2) Runoff Variability (RV) index,
225 the standard deviation of simulated runoff to the standard deviation of precipitation
226 (Sankarasubramanian and Vogel, 2003).

227 **3 Parameter regionalization procedure**

228 The following sections describe the workflow for the MWBM calibration and regionalization
229 (illustrated in Figure 3). The MWBM parameter sensitivities from the FAST analysis were
230 evaluated across the CONUS. The spatial patterns and magnitudes of parameter sensitivities
231 were used to organize the 109,951 HRUs into hydrologically similar regions referred to in the
232 paper as calibration regions. During the initial streamgauge selection, potential streamgages were
233 identified for use in the grouped MWBM calibration. These selected streamgages then were
234 individually calibrated. Using a number of selection criteria, a final set of calibration gages were
235 derived within each calibration region. The grouped MWBM calibration produced an ‘optimal’
236 set of MWBM parameters for each calibration region by evaluating simulated MWBM variables
237 converted to Z-scores.

238 *Figure 3. Schematic flowchart of the parameter regionalization procedure described in Section*
239 *3: Parameter sensitivities (3.1), Calibration regions (3.2), Initial streamgauge selection (3.3),*
240 *and Grouped streamgauge calibration (3.4).*

241 **3.1 Parameter sensitivities**

242 The relative sensitivities derived from the FAST analysis using the RR and RV indices at each of
243 the 109,951 HRUs across the CONUS were scaled so that the five MWBM parameter
244 sensitivities derived for each HRU summed to 100 (Fig. 4). RR (Fig. 4a) is most sensitive to the
245 parameter *Drofac* in regions where MWBM runoff is not dominated by snowmelt and orographic
246 precipitation, such as arid and sub-tropical areas of the CONUS. MWBM parameters that

247 control snowpack accumulation and melt (*Meltcoef*, *Tsnow*, and *Train*) are more important to the
248 RR in the extensive mountain ranges in the Western CONUS, and northerly latitudes around the
249 Great Lakes and in the Eastern CONUS. The RR indicates the highest sensitivity to the *Rfactor*
250 parameter in mountainous areas of the CONUS and areas of the West Coast, and moderate to
251 high sensitivity in areas where the sensitivity of RR to *Drofac* is low. *Tsnow*, *Train*, and
252 *Meltcoef* all share similar patterns across the CONUS. The spatial variability of the sensitivity of
253 RR to *Meltcoef* indicates different physical mechanisms controlling *Meltcoef* parameter influence
254 on RR in different areas of the CONUS. In the Western CONUS, the sensitivity of RR to
255 *Meltcoef* is greatest in mountainous areas that accumulate and hold snowpack through the late
256 spring, such as the Rocky Mountains, Cascade, and Sierra Nevada mountain ranges. In the
257 Eastern and Midwestern CONUS, the sensitivity of RR to *Meltcoef* is greatest for HRUs with
258 more northerly latitudes.

259 *Figure 4. Relative sensitivity of the (a) Rainfall Ratio (RR) and (b) Runoff Variability (RV)*
260 *indices to Monthly Water Balance Model parameters.*

261 The spatial patterns of sensitivities of RV to the five MWBM parameters (Fig. 4b) show both
262 similarities and deviations from the patterns shown in the RR maps. For the central part of the
263 CONUS, the relative sensitivity for the parameter *Drofac* is high for both indices, and low for the
264 parameter *Rfactor* for both indices. *Meltcoef*, *Tsnow*, and *Train* share the same relations between
265 higher sensitivity and higher elevation (primarily in the western part of the CONUS), and higher
266 sensitivity and more northerly latitude (primarily in the eastern half of the CONUS) for both
267 indices. However, *Drofac* and *Rfactor* show distinctly different patterns of relative sensitivities
268 for the eastern part of the CONUS for RV as compared to RR. The other three parameters
269 follow the same general spatial patterns for RV as compared to RR, but with greater fine-scale
270 spatial variation and patchiness. The differences between the spatial distributions of the
271 sensitivities between the two indices highlight that applying SA to different model outputs can
272 generate different levels of sensitivities for each parameter. In addition, the choice of objective
273 function or model output for which to measure parameter sensitivity is important, as parameter
274 sensitivities will differ depending on whether a user evaluating measures of magnitude, the
275 variability of distribution, or timing (Krause et al., 2005; Kapangaziwiri et al, 2012).

276 Figure 5 illustrates the variability of parameter sensitivities between NHDPlus regions 08 (Lower
277 Mississippi) and 14 (Upper Colorado) (see Fig. 2) for the RR and RV indices, and between the
278 RR and RV within a single region. The Lower Mississippi and Upper Colorado NHDPlus
279 regions have a similar number of HRUs (4,449 and 3,879, respectively) and cover a similar area
280 (26,285 and 29,357 km², respectively). The Lower Mississippi region has homogenous
281 topography, with humid, subtropical climate, while the Upper Colorado region has highly
282 variable topography, and thus highly variable climatic controls on hydrologic processes. For the
283 Lower Mississippi region only one parameter dominates modeled RV variance (*Rfactor*, Fig. 5a)
284 and modeled RR variance (*Drofac*, Fig. 5c). In contrast, for the Upper Colorado River region
285 several parameters influence RV variability (*Drofac*, *Rfactor* and *Meltcoef*, Fig. 5b) and RR
286 variability (*Drofac* and *Meltcoef*, Fig. 5d). In the Lower Mississippi Region the amount of
287 snowfall is negligible, so the three parameters that control snowfall and snowpack accumulation
288 in the MWBM have a negligible effect on the volume and variability of simulated total runoff.
289 The *Rfactor* parameter controls almost all of the variance for the RV in the Lower Mississippi
290 region. In humid, sub-tropical hydroclimatic regimes of the CONUS, peak runoff is coincident
291 with peak precipitation, which is significant because these periods are when the surplus runoff is
292 greatest. In the Upper Colorado, peak runoff is not coincident with peak precipitation, and the
293 MWBM snow parameters have more control in modulating the variability and timing of runoff
294 from snowmelt in the higher elevation HRUs. The comparison of the parameter sensitivities for
295 these two regions illustrates how variable parameter sensitivities differ by region (i.e. different
296 climatic and physiographic regions) and components of model response (i.e. volume and
297 variability).

298 *Figure 5. Parameter sensitivities of Runoff Variability (RV; a-b) and Runoff Ratio (RR; c-d)*
299 *indices for Monthly Water Balance Model parameters in the Lower Mississippi (R08) and*
300 *Upper Colorado (R14).*

301 **3.2. Calibration regions**

302 The spatial patterns and magnitudes of parameter sensitivities across the CONUS were used as a
303 basis for organizing HRUs into hydrologically similar regions for parameter regionalization
304 through MWBM calibration. This idea is rooted in the hypothesis that geographically proximate

305 HRUs share similar forcings and conditions, and thus will behave similarly. This application
306 uses similarity in SA results as a basis for organization, rather than similarity in physiographic
307 characteristics. The derived regions are subsequently used to simplify model calibration across
308 the CONUS and provide a basis for the transfer and application of parameters to ungaged areas.

309 The parameter sensitivities derived from the RR were used to organize the HRUs into two
310 independently-derived calibration regions; the first derived by identifying HRUs with unique
311 combinations of the order of parameter sensitivities to the RR (highest parameter sensitivities to
312 lowest, i.e. 1-*Drofac* (78%), 2-*Rfactor* (16%), 3-*Meltcoef* (5%), 4-*Tsnow* (1%), 5-*Train* (1%)),
313 and the second classification based upon identifying HRUs with unique sets of parameters whose
314 sensitivities exceeded a specified threshold of parameter sensitivity (i.e. only *Drofac*, *Rfactor*,
315 *Meltcoef* using a 5% threshold in the first classification example). The purpose of the first
316 classification was to delineate regions of similar model response or behavior based on the order
317 of importance of the MWBM parameters to the RR for each HRU. This classification identified
318 16 distinct regions of HRUS across the CONUS based on the order of the parameter sensitivities
319 of the five parameters (derived using the RR index). Sizes of these regions ranged from 94 km²
320 to almost 2 million km². The second classification delineated regions with an identical set of the
321 most important parameters to the RR based on parameters whose sensitivities exceeded a 5%
322 threshold. This step identified 12 regions of HRUs with unique combinations of parameter
323 sensitivities exceeding 5%. There has been progress in providing quantitative thresholds for the
324 identification of sensitive and non-sensitive parameters for hydrologic modelers (Tang et al.,
325 2007), but no definitive consensus yet exists. Therefore a 5% threshold was used based on visual
326 delineation of major physiographic features such as mountain ranges across the CONUS. The
327 sizes of this second group of regions ranged from 94 km² to more than 15 million km². Maps of
328 the two groupings of HRUS were intersected to create a total of 49 regions across the CONUS.
329 NHDPlus region and sub-region boundaries, proximity, and significant topographic divides were
330 used to further divide the groups into 159 geographically unique calibration regions across the
331 CONUS. The lack of streamgages available in some regions, especially areas with arid and
332 semi-arid climates, necessitated merging regions together. Calibration regions that contained
333 less than 3 streamgages from the 8,410 gages present in the Geospatial Fabric (see section 3.3)
334 were combined with the proximate and most similar group which shared the most similar

335 parameter sensitivities (both order and magnitude), resulting in 110 calibration regions across
336 the CONUS (Fig. 6). Within each region the FAST results for both the RR and RV indices were
337 used to determine which parameters to calibrate. Within each region, parameters with a median
338 parameter sensitivity of 5% for the RR and RV among the region's HRUs were selected for
339 group calibration. Parameters not shown as sensitive were kept at the default value for the
340 group.

341 *Figure 6. Final 110 Monthly Water Balance Model calibration regions differentiated by colors.*
342 *A subset of streamgages within each calibration region were calibrated in a group-wise*
343 *fashion to produce a single optimized parameter set for the entire region (Fig. 3).*

344 **3.3 Initial streamgage selection**

345 The initial set of streamgages used for testing in the MWBM calibration procedures was selected
346 from 8,410 streamgages identified in the Geospatial Fabric (Fig. 7). The Geospatial Fabric
347 includes reference and non-reference streamgages from the Geospatial Attributes of Gages for
348 Evaluating Streamflow dataset (GAGES, Falcone et al., 2010). Of the 8,410 streamgages in the
349 Geospatial Fabric, 1,864 were identified as having reference-quality data with at least 20 years of
350 record. These reference quality streamgages were judged to be largely free of human alterations
351 to flow (Falcone et al., 2010). In the current study, reference quality was not considered in the
352 initial streamgage selection because the 20 years of record was considered too restrictive.
353 Therefore a subset of the 8,410 streamgages was selected for initial testing in the MWBM
354 calibration procedures based on the following criteria:

- 355 (1) Remove streamgages with less than 10 years of total measured streamflow (120 months)
356 within the time period 1950 – 2010.
- 357 (2) Remove streamgages with a drainage area defined by the Geospatial Fabric that are not
358 within 5% of the USGS National Water Information System (NWIS) reported drainage
359 area (U.S. Geological Survey, 2014). This eliminated many of the streamgages with
360 smaller drainage areas due to the resolution of the Geospatial Fabric.
- 361 (3) Remove streamgages that did not have at least 75% of its drainage area contained within
362 a single calibration region.

363 These criteria resulted in 5,457 potential streamgages for testing in the MWBM calibration
364 procedures (Fig. 7). Streamflow at these streamgages was aggregated and converted from daily
365 (cubic feet/second) to a monthly runoff depth (mm) (streamflow per unit area).

366 *Figure 7. Streamgages tested in the study. GF notes geospatial fabric for national hydrologic*
367 *modeling (Viger and Bock, 2014).*

368 **3.4 Monthly Water Balance Model calibration**

369 Two automated calibration procedures were implemented to produce an ‘optimal’ set of MWBM
370 parameters for each calibration region. The first procedure, Individual Streamgage Calibration,
371 calibrated each of the 5,457 streamgages individually. Results from the individual calibrations
372 were used to further filter the streamgages within the second procedure, Grouped Streamgage
373 Calibration, which calibrated selected streamgages together by calibration region.

374 **3.4.1 Individual streamgage calibration**

375 The first calibration procedure was an automated process that individually calibrated each of the
376 5,457 streamgages from the initial streamgage selection with measured streamflow (U.S.
377 Geological Survey, 2014). Results from these individual streamgage calibrations quantified the
378 ‘best’ performance of the MWBM at each gage, providing a ‘baseline’ measure for evaluation.

379 The Shuffled Complex Evolution (SCE) global-search optimization algorithm (Duan et al., 1993)
380 has been frequently used as an optimization algorithm in hydrologic studies (Hay et al., 2006;
381 Blasone et al. 2007; Arnold et al., 2012), including previous studies with the MWBM (Hay and
382 McCabe, 2010). Further details can be found in Duan et al. (1993). SCE was used to maximize a
383 combined objective function based on: (1) Nash-Sutcliffe Efficiency (NSE) coefficient using
384 measured and simulated monthly runoff and (2) NSE using natural log-transformed measured
385 and simulated runoff (logNSE), using the entire period of record for each streamgage. The NSE
386 measures the predictive power of the MWBM in matching the magnitude and variability of the
387 measured and simulated runoff (Nash and Sutcliffe, 1970). The NSE coefficient ranges from $-\infty$
388 to 1, with 1 indicating a perfect fit, and values less than 0 indicating that measured mean runoff
389 is a better predictor than model simulations. The NSE has been shown to give more weight to
390 the larger values in a time series (peak flows) at the expense of lower values (low flows)

391 (Legates and McCabe, 1999), so the logNSE was incorporated into the objective function to give
392 weight to lowflow periods (Tekleab et al., 2011).

393 **3.4.2 Grouped streamgage calibration**

394 The second calibration procedure was an automated process that calibrated groups of
395 streamgages together for each calibration region to derive a single set of MWBM parameters
396 (Table 1) for each calibration region (Fig. 6). The NSE and logNSE values from the individual
397 streamgage calibrations (described in the previous section) were used to identify streamgages
398 that should not be used for grouped streamgage calibration. If the individual streamgage
399 calibration was not ‘satisfactory’, then it was felt that it would not provide useful information for
400 the grouped streamgage calibration procedure.

401 Satisfactory individual streamgage calibrations were identified with the following procedure:

- 402 (1) Eliminate all streamgages with NSE values < 0.3 .
- 403 (2) If the number of remaining streamgages for a given calibration region is > 10 , then
404 eliminate all streamgages with NSE < 0.5 .
- 405 (3) If the number of streamgages for a given calibration region is > 25 , then eliminate all
406 streamgages with $NSE_{log} < 0$.
- 407 (4) If the number of remaining streamgages for a calibration region is < 5 , check to see if any
408 of the eliminated streamgages were reference streamgages (as defined in Falcone et al, 2010),
409 then add the reference streamgages back in if the NSE value > 0.0 . Reference streamgages are
410 USGS streamgages deemed to be largely free of anthropogenic impacts and flow modifications
411 (Falcone et al., 2010; Kiang et al., 2013).

412 These criteria, while somewhat arbitrary, were chosen so that no calibration region had less than
413 5 streamgages for the grouped streamgage calibration. Using the above criterion, of the 5,457
414 streamgages individually calibrated, 3,125 remained as candidates for the grouped streamgage
415 calibration procedure.

416 The grouped streamgauge calibration procedure used the SCE global-search optimization
 417 algorithm with a multi-term objective function (Eq. 1). Measured and simulated values for
 418 selected streamgages contained within a calibration region were scaled to Z-scores to remove
 419 differences in magnitudes between streamgages (Eq. 2). The multi-term objective function
 420 minimized the sum of the absolute differences between Z-scores from four measured and
 421 simulated time series: mean monthly runoff (MMO, MMS), monthly runoff (MO, MS), annual
 422 runoff (AO, AS) (U.S. Geological Survey, 2014), and monthly snow water equivalent (SO, SS))
 423 for all selected streamgages within a given calibration region:

$$424 \quad \min \sum_{i=1}^n [3|MMO_i - MMS_i| + |MO_i - MS_i| + |AO_i - AS_i| + 0.5|SO_i - SS_i|] \quad (\text{Eq.1})$$

425

$$\text{where } \begin{cases} 0 & \text{if } 0.75 < SO_i - SS_i < 1.25 \\ |SO_i - SS_i| & \text{if } SS_i < SO_i^{0.75} \\ |SO_i - SS_i| & SS_i > SO_i^{1.25} \end{cases}$$

426 The measured and simulated Z-scores were calculated as:

$$427 \quad Z = (x-u)/\sigma \quad (\text{Eq. 2})$$

428 where x is the time-series value, u is the mean, and σ the standard deviation of the measured and
 429 simulated variable.

430 ‘Measured’ SWE was determined for each HRU from the Snow Data Assimilation System
 431 (SNODAS; National Operational Hydrologic Remote Sensing Center, 2004) and included a +/-
 432 25% error bound. The unconstrained automated calibration (without a restriction on SWE) led to
 433 unrealistic sources of snowmelt in the summer that enhanced the low-flow simulations. The 25%
 434 error bound is arbitrary; calibrating to the actual SNODAS SWE values was found to be too
 435 restrictive, but adding this error bound to the SWE values resulted in better overall runoff
 436 simulations. The absolute difference of the simulated SWE Z-scores that were within +/- 25% of
 437 the measured SWE Z-score were designated as 0. Otherwise, the absolute difference was
 438 computed between the simulated SWE Z-score and either the upper or lower bounds (Eq. 1).

439 The grouped calibration procedure was run for all 110 calibration regions. For each calibration
 440 region the seasonal adjustment parameters and the sensitive parameters (identified by the FAST

441 analysis -- section 3.1) were calibrated; parameters deemed not sensitive (parameter sensitivity <
442 5% of total variance) were set to their default values (see Table 1). The entire period of the
443 streamflow record for each streamgauge was split by alternating years. After calibration, mean
444 monthly measured and simulated Z-scores for runoff at all selected streamgages within a
445 calibration region were compared.

446 Figure 8 shows an example of the graphic used to evaluate the measured and simulated mean
447 monthly Z-scores for 21 streamgages selected for the region located in the Tennessee River
448 calibration region (part of NHDPlus Region R06 in Fig. 2); the orange, red, and black dots
449 indicate calibration, evaluation, and the entire period of record, respectively. A tight grouping
450 around the one-to-one line indicates good correspondence between measured and simulated Z-
451 scores. Points closer to the upper right corner of each plot represent high-flow periods. Points
452 closer to the lower left corner of the plot represent low-flow periods. Streamgages within a
453 calibration region were assigned the same parameter values; therefore streamgages that plotted
454 outside (two standard deviations) of the one-to-one line were considered to not be representative
455 of the calibration region, and the calibration procedure for that calibration region was repeated
456 without those streamgages.

457 *Figure 8. Measured versus simulated mean monthly Z-scores for the Tennessee River*
458 *calibration region (see Fig. 10b for location). Orange is calibration, red is evaluation, and*
459 *black is all years.*

460 The goal of the second calibration procedure was to find a single parameter set for each
461 calibration region. Past applications of the MWBM (Wolock and McCabe, 1999, McCabe and
462 Wolock, 2011a) used a single set of fixed MWBM parameters for the entire CONUS. Many of
463 the streamgages included in the second calibration procedure could be affected by significant
464 anthropogenic effects; the seasonal adjustment factors, calibrated at each individual streamgauge,
465 could account for these effects and result in satisfactory NSE values. Streamgages that were
466 removed due to poor performance in the second calibration were assumed to have anthropogenic
467 effects not consistent with the streamgages that plotted along the one-to-one line. Poor
468 performance may result because the MWBM fails to reliably simulate runoff for a watershed
469 because of model limitations (i.e. not including all important hydrologic processes), but the

470 calibration regions are assumed to be homogeneous based on the FAST analysis. Therefore it is
471 assumed that if some of the streamgages within a region have satisfactory results, then the
472 MWBM is able to simulate runoff in that region.

473 **4 MWBM calibration region results**

474 **4.1 Individual streamgage calibration results**

475 The individual streamgage calibrations provided information regarding: (1) the potential
476 suitability of a given streamgage for inclusion in a grouped calibration, and (2) a ‘baseline’
477 measure for evaluation of the grouped calibration results. Reference and non-reference
478 streamgages were considered in this application; if the runoff at a streamgage could not be
479 calibrated individually to a ‘satisfactory’ level (based on criterion outlined in section 3.4.2), then
480 it was felt that it would not provide useful information for the grouped streamgage calibration
481 procedure. Figure 9 shows the NSE (Fig. 9a) and logNSE (Fig. 9b) coefficients from the
482 individual streamgage calibrations for the CONUS. Scattered throughout the CONUS are NSE
483 and logNSE values less than 0.0 (triangles in Fig. 9). These poor results are likely streamgages
484 with poor streamflow records, either due to measurement error or anthropogenic effects (dams,
485 water use, etc.).

486 *Figure 9. Individual streamgage calibration results: (a) Nash-Sutcliffe Efficiency (NSE)*
487 *coefficient and (b) log of the NSE (logNSE).*

488 **4.2 Grouped streamgage calibration results**

489 **4.2.1 Mean monthly z-scores**

490 Figure 10a shows a scatterplot of measured versus simulated mean monthly Z-scores for runoff,
491 similar to Figure 8, but based on all available years (the black dots in Fig. 8) for all the final
492 calibration streamgages (1,575 streamgages). Four regions are highlighted to illustrate the
493 monthly variability in MWBM results across the CONUS (see Fig. 10b for locations). The four
494 regions are: New England (67 streamgages, red); Tennessee River basin (21 streamgages,
495 orange); Platte Headwaters (15 streamgages, blue); and Pacific Northwest (33 streamgages,
496 green) (Fig. 10b).

497 *Figure 10. (a) Measured versus simulated mean monthly Z-scores for runoff at all streamgages*
498 *and (b) location of highlighted streamgages for four calibration regions: New England (67*
499 *streamgages, red); Tennessee River (21 streamgages, orange); Platte Headwaters (15*
500 *streamgages, blue); and Pacific Northwest (33 streamgages, green).*

501 In Fig. 10a, three of the regions (New England, Tennessee River, and Pacific Northwest), show
502 simulated Z-scores that correspond favorably to measured Z-scores for each of the twelve
503 months, including periods of low and high runoff. These regions represent marine or humid
504 climates with homogenous physio-climatic conditions and an even spatial distribution of
505 streamgages, where models should be expected to perform well (see Fig. 9) There is a higher
506 variability in model results for the high-flow months (May - June) for streamgages within the
507 Platte Headwaters (Fig. 10a; blue dots) than for low-flow months. This variability may be
508 related to factors controlling the magnitude and timing of snow melt runoff (Fig. 9).

509 For each calibration streamgage, a set of four months were identified that represent different
510 parts of the measured mean monthly hydrograph (highest- and lowest- flow month and the two
511 median-flow months). The measured and simulated mean monthly streamflow Z scores
512 corresponding to the four months are plotted as cumulative frequencies (Fig. 11) to compare how
513 well the simulated Z scores matched measured Z scores for different parts of the hydrograph
514 over the entire set of calibration gages. For the highest-flow, there is an under-estimation of
515 runoff, with the greatest divergence between the two distributions in the middle to lower half of
516 the distribution (Fig. 11a). For the median-flow, the measured and simulated Z scores are well
517 matched. For the 10 lowest-flow, simulated Z scores are greater than measured Z scores, with the
518 greatest divergence between the two distributions in the middle to upper half of the distribution
519 (Fig. 11c).

520 *Figure 11. Z-score cumulative frequency for (a) highest-, (b) median-, and (c) lowest-flow*
521 *months.*

522 The median Z-score errors (simulated - measured) by region for the (a) highest-, (b) median-,
523 and (c) lowest-flows are shown in Figure 12. The largest errors are for the highest-flows (Fig.
524 12a). The MWBM simulations under-estimate the highest flows for much of the CONUS. The

525 errors for median-flows are fairly uniform and consistent across the CONUS (Fig. 12b), with a
526 median error close to 0. For the lowest-flow months the MWBM over-estimates low flows for a
527 large portion of the Midwest (Fig. 12c).

528 *Figure 12. Z-score error (simulated - measured) for (a) highest-, (b) median-, and (c) lowest-*
529 *flow months.*

530 **4.2.2 Nash-Sutcliffe efficiency**

531 Figure 13 compares the NSE from the individual streamgage calibrations (gageNSE) with the
532 grouped calibrations (groupNSE) for all final streamgages used in the second calibration
533 procedure. NSE values > 0.75 (dashed line) and > 0.5 (solid line) indicate very good and
534 satisfactory results (Moriassi et al., 2007). Overall, most NSE values fall above the 0.5 NSE
535 threshold of satisfactory performance (median of gageNSE and groupNSE = 0.76). The gageNSE
536 values are used here as a ‘baseline’ for evaluation of the groupNSE results. The groupNSE
537 values were not expected to be greater than the gageNSE values since (1) NSE was not used as
538 an objective function in the grouped calibration, and (2) grouped calibrations found the ‘best’
539 parameter set for a set of streamgages versus an individual streamgage. Figure 13 shows an equal
540 distribution of NSE values around the one-to-one line, indicating that the grouped calibration
541 provided additional information over the individual streamgage calibrations (cases where
542 groupNSE are greater than gageNSE in Fig. 13). The difference between the gageNSE and
543 groupNSE becomes larger as the NSE values decrease, reflecting the increasing uncertainty in
544 the grouped calibrations in areas with lower gageNSE values.

545 *Figure 13. Nash Sutcliffe Efficiency from individual (gageNSE) and grouped (groupNSE)*
546 *calibration. Calibration regions in New England (67 streamgages, red); Tennessee River*
547 *(21 streamgages, orange); Platte Headwaters (15 streamgages, blue); and Pacific Northwest*
548 *(33 streamgages, green) are highlighted (see Fig. 10b for location).*

549 Four regions are highlighted in Fig. 13 to illustrate the variability of NSE across the CONUS
550 (see Fig. 10b for locations). The highlighted regions in New England (red), Tennessee River
551 (orange), and Pacific Northwest (green), show good groupNSE and gageNSE results. Four of

552 the 15 streamgages in the Platte Headwaters (blue) have groupNSE values ≤ 0.5 . This is
553 probably related to simulation error during the snowmelt period (May - June, Fig. 10a).

554 Figure 14 shows the median groupNSE by calibration region for the CONUS. The pattern is very
555 similar to that shown for the individual streamgage calibration results in Fig. 9a and highlights
556 the problem areas shown in Fig. 12.

557 *Figure 14. Median Nash Sutcliffe Efficiency (NSE) of streamgages used for calibration by*
558 *calibration region.*

559

560 **5 Discussion**

561 This study presented a parameter regionalization procedure for calibration of the MWBM,
562 resulting in an application that can be used for simulation of hydrologic variables for both gaged
563 and ungaged areas in the CONUS. The regionalization procedure grouped HRUs on the basis of
564 similar sensitivity to five model parameters. Parameter values and model uncertainty
565 information within a group was then passed from gaged to ungaged areas within that group.

566 **5.1 Regionalized parameters**

567 Results from this study indicate that regionalized parameters can be used to produce satisfactory
568 MWBM simulations in most parts of the CONUS (Fig. 13). Despite the differences between the
569 individual streamgage calibration and grouped calibration, Figure 13 illustrates that the grouped
570 calibration strategy, which focused only on sensitive parameters, can provide just as much
571 information as the individual streamgage calibration with no constraints on the parameter
572 optimization other than the default ranges. The MWBM is a simple hydrologic model as it has
573 minimal parameters, which are conceptual in nature (not physically based). It may be that this
574 type of model is best for regionalization when parameter sensitivity can be identified and HRU
575 behavior can be classified by a small number of clearly defined spatial groups. More
576 complicated models with many more interactive parameters may not respond as well to this
577 simple type of regionalization; more parameters may lead to more parameter interaction and
578 situations of equifinality which might confuse the analysis.

579 The adjustments of precipitation and temperature parameters for the individual streamgage
580 calibrations accounted for local errors such as rain gage under catch of precipitation. In addition
581 these climate adjustments also account for local anthropogenic effects on streamflow (e.g. dams,
582 diversions) since streamgages were not screened for these effects prior to individual streamgage
583 calibration. In the grouped streamgage calibrations, the same precipitation and temperature
584 adjustments are applied at every streamgage within the calibration region, making these climate
585 adjustments more of a regional adjustment and producing more of a ‘reference’ condition for
586 each calibration region.

587 **5.2 Parameter sensitivities and dominant process**

588 The MWBM parameter sensitivities varied by hydroclimatic index (RR and RV) and across the
589 CONUS (Fig. 3). The parameter sensitivity patterns give an indication of dominant hydrologic
590 processes based on MWBM. The dominant process can be seasonal and MWBM performance
591 may be enhanced by extending the use of SA along the temporal domain to identify and
592 temporally vary the parameters that are seasonally important to the MWBM. For example, error
593 in peak flow months is the primary cause for poor model performance in the Platte Headwaters
594 (Fig. 9). For the Platte Headwaters, the final parameter set performed well for simulated Z-
595 scores for the regionalized low- and median-flow conditions (Fig. 9a, July through April), but
596 was not able to replicate measured mean monthly flows for May and June. In this case, the
597 dominant processes controlling hydrologic behavior change with season and the parameters
598 controlling the dominant response may have to change accordingly (Gupta et al., 2008; Reusser
599 et al., 2011).

600 **5.3 Model accuracy**

601 The pattern of MWBM accuracies shown in Fig. 8 and 14 are similar to those shown by Newman
602 et al. (2015; Fig. 5a) in which a daily time-step hydrologic model was calibrated for 671 basins
603 across the CONUS. Our study and the Newman et al. (2015) study both indicate the same
604 ‘problem areas’ with the poorest performing basins generally being located in the high plains and
605 desert southwest. Newman et al. (2015) attributed variation in model performance by region to

606 spatial variations in aridity and precipitation intermittency, contribution of snowmelt, and runoff
607 seasonality.

608 The inferior MWBM results in the ‘problem areas’ can be attributed to multiple factors which
609 likely include inadequate hydrologic process representation and errors in forcing data (e.g.
610 climate data), and/or measured streamflow. Archfield et al. (2015) state that the performance of
611 continental-domain hydrologic models is considerably constrained by inadequate model
612 representation of dominant hydrologic processes. For example, the simplicity of the MWBM
613 presents limitations on the representation of deeper groundwater reservoirs, gaining and losing
614 stream reaches, simplistic AET, and the effects of surface processes (infiltration and overland
615 flow) that need to be represented at finer time steps than monthly.

616 The dominant hydrologic processes in the ‘problem areas’ appear to be poorly represented at the
617 daily (Newman et al., 2015) and monthly time steps. This may be due to inadequate forcing
618 data, the quality of which ‘is paramount in hydrologic modeling efforts’ (Archfield et al., 2015)
619 and/or the lack of ‘good’ reference streamflow data for calibration and evaluation. Both surely
620 play a role and emphasize the need for incorporation of additional datasets so that calibration and
621 evaluation of intermediate states in the hydrologic cycle are examined.

622 **6 Conclusions**

623 A parameter regionalization procedure was developed for the CONUS that transferred parameter
624 values from gaged to ungaged areas for a MWBM. The FAST global-sensitivity algorithm was
625 implemented on a MWBM to generate parameter sensitivities on a set of 109,951 HRUs across
626 the CONUS. The parameter sensitivities were used to group the HRUs into 110 calibration
627 regions. Streamgages within each calibration region were used to calibrate the MWBM
628 parameters to produce a regionalized set of parameters for each calibration region. The
629 regionalized MWBM parameter sets were used to simulate monthly runoff for the entire
630 CONUS. Results from this study indicate that regionalized parameters can be used to produce
631 satisfactory MWBM simulations in most parts of the CONUS.

632 The best MWBM results were achieved simulating low- and median-flows across the CONUS.
633 The high-flow months generally showed lower skill levels than the low- and median-flow

634 months, especially for regions with dominant seasonal cycles. The lowest MWBM skill levels
635 were found in the high plains and desert southwest and can be attributed to multiple factors
636 which likely include inadequate hydrologic process representation and errors in forcing data
637 and/or measured streamflow. Calibration and evaluation of intermediary fluxes and states in the
638 MWBM through additional measured datasets may help to improve MWBM representations of
639 these model states by helping to constrain parameterization to measured values.

640 **7 Acknowledgments**

641 This research was financially supported by the U.S. Department of Interior South Central
642 Climate Science Center (<http://southcentralclimate.org/>), U.S. Environmental Protection Agency
643 Office of Water, and the U.S. Geological Survey WaterSMART initiative. This paper is a
644 product of discussions and activities that took place at the USGS John Wesley Powell Center for
645 Analysis and Synthesis (<https://powellcenter.usgs.gov/>). Further project support was provided
646 by the Jeff Falgout of the USGS Core Science Systems (CSS) Mission Area. Any use of trade,
647 product, or firm names is for descriptive purposes only and does not imply endorsement by the
648 U.S. Government.

649

650

651

652

653

654

655

656

657

658

659

660

661 **8 References**

662 Adam, J.C., and Lettenmaier, D.P.: Bias correction of global gridded precipitation for solid
663 precipitation undercatch, *J. Geophys. Res.*, 108, 1-14, doi:10.1029/2002JD002499, 2003.

664 Ali, G., Tetzlaff, D., Soulsby, C., McDonnell, J.J., and Capell, R.: A comparison of similarity
665 indices for catchment classification using a cross-regional dataset, *Adv. Water Resources*, 40,
666 11-22, <http://dx.doi.org/10.1016/j.advwatres.2012.01.008>, 2012.

667 Archfield, S.A., Clark, M., Arheimer, B., Hay, L.E., Farmer, W.H, McMillan, H., Seibert, J.,
668 Kiang, J.E., Wagener, T., Bock, A., Hakala, K., Andressian, V., Attinger, S., Viglione, A.,
669 Knight, R.R., and Over, T.: Accelerating advances in continental domain hydrologic modeling,
670 *Water Resour. Res.*, 51, 10078-10091, doi: 10.1002/2015WR017498, 2015.

671 Arnold, J.G., Moriasi, D.N., Gassman, P.W., Abbaspour, K.C., White, M.J., Srinivasan, R.,
672 Santhi, C., Harmel, R.D., van Griensven, A., Van Liew, M.W., Kannan, N., and Jha, M.K.:
673 SWAT: Model Use, Calibration and Validation, *T. ASABE*, 55(4), 1491-1508, doi:
674 10.13031/2013.42256, 2012.

675 Blasone, R.S., Madsen, H., and Rosbjerg, D.: Parameter estimation in distributed hydrological
676 modelling: comparison of global and local optimisation techniques, *Nord. Hydrol.*, 34,451-476,
677 doi:10.2166/nh.2007.024, 2007.

678 Blodgett, D.L., Booth, N.L., Kunicki, T.C., Walker, J.L., and Viger, R.J.: Description and
679 Testing of the Geo Data Portal: A Data Integration Framework and Web Processing Services for
680 Environmental Science Collaboration. US Geological Survey, Open-File Report 2011-1157, 9
681 pp., Middleton, WI, USA, 2011.

682 Blöschl, G., and Sivapalan, M.: Scale issues in hydrological modeling: a review, *Hydrol.*
683 *Process.*, 9, 251-290, doi:10.1002/hyp.3360090305, 1995.

684 Blöschl, G., Sivapalan, M., Wagener, T., Viglione, A., and Savenije, H (Eds.): *Runoff*
685 *Prediction in Ungauged Basins: Synthesis across Processes, Places, and Scales*. Cambridge
686 University Press, Cambridge, England, 2013.

687 Clark, M.P., and Slater, A.G.: Probabilistic Quantitative Precipitation Estimation in Complex
688 Terrain, B. Am. Meterol. Soc., 7, 3-2, doi: <http://dx.doi.org/10.1175/JHM474.1>, 2006.

689 Cukier, R.I., Fortuin, C.M., Shuler, K.E., Petschek, A.G, and Schaibly, J.H: Study of sensitivity
690 of coupled reaction systems to uncertainties in rate coefficients 1, J. Chem. Phys., 59(8), 3873-
691 3878, doi:10.1063/1.1680571, 1973.

692 Cukier, R.I., Schiably, J.H., and Shuler, K.E: Study of sensitivity of coupled reaction systems to
693 uncertainties in rate coefficients 3, J. Chem. Phys., 63(3), 1140-1149, doi:1063/1.431440, 1975.

694 Cuo, L., Giambelluca, T.W., and Ziegler, A.D: Lumped parameter sensitivity analysis of a
695 distributed hydrological model within tropical and temperate catchments, Hydrol. Process.,
696 25(15), 2405-2421, doi:10.1002/hyp.8017, 2011.

697 Duan, Q., Gupta, V.K., and Sorooshian, S.: A shuffled complex evolution approach for effective
698 and efficient optimization, J. Optimiz. Theory App., 76, 501-521, doi:10.1007/BF00939380,
699 1993.

700 Falcone, J.A., Carlisle, D.M., Wolock, D.M., and Meador, M.R.: GAGES: A stream gage
701 database for evaluating natural and altered flow conditions in the conterminous United States,
702 Ecology, 91, p. 621, A data paper in Ecological Archives E091-045-D1, available at
703 <http://esapubs.org/Archive/ecol/E091/045/metadata.htm> (last accessed 15 November 2012),
704 2010.

705 Farnsworth, R.K., Thompson, E.S., and Peck, E.L.: Evaporation Atlas for the Contiguous 48
706 United States, NOAA Technical Report NWS 33, 41 pp., National Oceanic and Atmospheric
707 Administration, Washington, D.C., 1982.

708 Groisman, P.Y., and Legates, D.R.: The accuracy of United States precipitation data, Bull. Am.
709 Meterol. Soc., 75(2), 215-227, doi: 10.1175/1520-0477(1994)075<0215:TAOUSP>2.0.CO;2,
710 1994.

711 Gupta, H.V., Wagener, T., Liu, Y.Q. Reconciling theory with observations: Elements of
712 diagnostic approach to model evaluation, *Hydrologic Processes*, 22, 3802-3813, doi:
713 10.1002/hyp.6989, 2008.

714 Guse, B., Reusser, D.E., and Fohrer, N.: How to improve the representation of hydrological
715 processes in SWAT for a lowland catchment - temporal analysis of parameter sensitivity and
716 model performance, *Hydrol. Process.*, 28(4), 2561-2670, doi:10.1002/hyp.9777, 2013.

717 Hay, L.E., Leavesley, G.H., Clark, M.P., Markstrom, S.L., Viger, R.J., and Umemoto, M.: Step-
718 wise multiple-objective calibration of a hydrologic model for a snowmelt-dominated basin, *J.*
719 *Am. Water Resour. A.*, 42(4), 877-890, doi:10.1111/j.1752-1688.2006.tb04501.x, 2006.

720 Hay, L.E., and McCabe, G.J.: Spatial Variability in Water-Balance Model Performance in the
721 Conterminous United States, *J. Am. Water Resour. Assoc.*, 38(3), 847-860, DOI:
722 10.1111/j.1752-1688.2002.tb01001.x, 2002.

723 Hay, L.E., and McCabe, G.J.: Hydrologic effects of climate change in the Yukon River Basin,
724 *Climate Change*, 100, 509-523, doi:10.1007/s10584-010-9805-x, 2010.

725 Kapangaziwiri, E., Hughes, D. A., and Wagener, T.: Constraining uncertainty in hydrological
726 predictions for ungauged basins in southern Africa, *Hydrol. Sci. J.*, 57, 1000–1019, 5
727 doi:10.1080/02626667.2012.690881, 2012.

728 Kiang, J.E., Stewart, D.W., Archfield, S.A., Osborne, E.B., and Eng, K.: A National Streamflow
729 Network Gap Analysis. U.S. Geological Survey, Scientific Investigative Reports 2013-5013, 94
730 pp., Reston, VA, USA, 2013.

731 Kirchner, J.W.: Getting the right answers for the right reasons: Linking measurements,
732 analyses, and models to advance the science of hydrology, *J. Hydrol.*, 42, W03S04,
733 doi:10.1029/2005WR004362, 2006.

734 Kokkonen, T.S., Jakeman, A.J., Young, P.C., and Koivusalo, H.J.: Predicting daily flows in
735 ungauged catchments: model regionalization from catchment descriptors at the Coweeta

736 Hydrologic Laboratory, North Carolina, *Hydrol. Process.*, 17, 2219-2238, doi:10.1002/hyp.1329,
737 2003.

738 Krause, P., Doyle, D. P., and Bäse, F.: Comparison of different efficiency criteria for
739 hydrological model assessment, *Adv. Geosci.*, 5, 89–97, doi:10.5194/adgeo-5-89-2005, 2005.

740 Legates, D.R., and McCabe, G.J.: Evaluating the use of “goodness-of-fit” Measures in
741 hydrologic and hydroclimatic model validation, *Water Resour. Res.*, 35(1), 233-241,
742 doi:10.1029/1998WR900018, 1999.

743 Maurer, E.P., Wood, A.W., Adam, J.C., Lettenmaier, D.P., and Nijssen, B.: A long-term
744 hydrologically-based data set of land surface fluxes and states for the conterminous United
745 States, *J. Climatol.*, 15, 3237-3251, [http://dx.doi.org/10.1175/1520-](http://dx.doi.org/10.1175/1520-0442(2002)015<3237:ALTHBD>2.0.CO;2)
746 [0442\(2002\)015<3237:ALTHBD>2.0.CO;2](http://dx.doi.org/10.1175/1520-0442(2002)015<3237:ALTHBD>2.0.CO;2), 2002.

747 McCabe, G.J., Hay, L.E., Bock, A., Markstrom, S.L., and Atkinson, R.D.: Inter-annual and
748 spatial variability of Hamon potential evapotranspiration model coefficients, *J. Hydrol.*, 521,
749 389-394, doi:10.1016/j.jhydrol.2014.12.006, 2015.

750 McCabe, G.J., and Markstrom, S.L.: A Monthly Water-Balance Model Driven By a Graphical
751 User Interface. U.S. Geological Survey Open-File Report 2007-1008, 12 pp., Reston, VA, USA,
752 2007.

753 McCabe, G.J., and Wolock, D.M.: Century-scale variability in global annual runoff examined
754 using a water balance model, *Int. J. Climatol.*, 31, 1739-1748, doi:10.1002/joc.2198, 2011a.

755 McCabe, G.J., and Wolock, D.M.: Independent effects of temperature and precipitation on
756 modeled runoff in the conterminous United States, *Water Resour. Res.*, 47, W1152,
757 doi:10.1029/2011WR010630, 2011b.

758 McManamay, R.A., Orth, D.J., Dolloff, C.A., and Frimpong, E.A: Regional Frameworks
759 applied to Hydrology: Can Landscape-based frameworks capture the hydrologic variability?,
760 *River Res. App.*, 28, 1325-1339, doi:10.1002/rra.1535, 2011.

761 Merz, R., and Blöschl, G.: Regionalisation of catchment model parameters, *J. Hydrol.*, 287, 95-
762 123, doi:10.1016/j.jhydrol.2003.09.028, 2004.

763 Moriasi, D.N, Arnold, J.G., Van Liew, M.W., Bingner, R.L., Harmel, R.D., and Vieth, T.L.:
764 Model Evaluation Guidelines for Systematic Quantification of Accuracy in Watershed
765 Simulations, *T. ASABE*, 50, 885-900, doi: 10.13031/2013.23153, 2007.

766 Nash, J.E., and Sutcliffe, J.V.: River flow forecasting through conceptual models Part I: a
767 discussion of principles, *J. Hydrol.*, 10, 282-290, doi:10.1016/0022-1694(70)90255-6, 1970.

768 National Operational Hydrologic Remote Sensing Center, Snow data Assimilation System
769 (SNODAS) Data Products at the NSIDC, 9/30/2003 through 6/13/2014, National Snow and Ice
770 Data Center, Boulder, Colorado, USA, <http://dx.doi.org/10.7265/N5TB14TC>, 2004.

771 Newman, A.J., Clark, M.P., Sampson, K., Wood, A., Hay, L.E., Bock, A., Viger, R.J., Blodgett,
772 D., Brekke, L., Arnold, J.R., Hopson, T., and Duan, Q.: Development of a large-sample
773 watershed-scale hydrometeorological data set for the contiguous USA: data set characteristics
774 and assessment of regional variability in hydrologic model performance, *Hydrol. Earth Syst. Sc.*,
775 19, 209-223, doi:10.5194/hess-19-209-2015, 2015.

776 Oudin, L., Andréassian, V., Perrin, C., Michel, C., and Le Moine, N.: Spatial proximity,
777 physical similarity, regression and ungaged catchments: a comparison of regionalization
778 approaches based on 913 French catchments, *Water Resour. Res.*, 44, 1-15,
779 doi:10.1029/2007WR006240, 2008.

780 Oudin, L., Kay, A., Andréassian, V., and Perrin, C.: Are seemingly physically similar
781 catchments truly hydrologically similar?, *Water Resour. Res.*, 46, W11558,
782 doi:10.1029/2009WR008887, 2010.

783 Oyler, J.W., Dobrowski, S.Z., Ballantyne, A.P., Klene, A.E., and Running, S.W.: Artificial
784 amplification of warming trends across the mountains of the western United States, *Geophys.*
785 *Res. Lett.*, 42, 153-161, doi:10.1002/2014GL062803, 2015.

786 Peel, M.C., Chiew, F.H.S., Western, A.W., and McMahon, T.A.: Extension of unimpaired
787 monthly streamflow data and regionalization of parameter values to estimate streamflow in
788 ungauged catchments. Report to National Land and Water Resources Audit, Center for
789 Environmental Application and Hydrology, University of Melbourne, Parkville, 2000.

790 R Core Team: R: A language and environment for statistical computing, R Foundation for
791 Statistical Computing, Vienna, Austria, 2013.

792 Reusser, D.: fast: Implementation of the Fourier Amplitude Sensitivity Test (FAST), R package
793 version, <http://CRAN.R-project.org/package=fast>, (last access: 9 April 2014), 2012.

794 Reusser, D., Buytaert, W., and Zehe, E.: Temporal dynamics of model parameter sensitivity for
795 computationally expensive models with the Fourier amplitude sensitivity test, *Water Resour.*
796 *Res.*, 47, W07551, doi:10.1029/2010WR009947, 2011.

797 Saltelli, A., Tarantola, S., and Campolongo, F.: Sensitivity analysis as an ingredient of
798 modeling, *Stat. Sci.*, 15, 377-395, 2000.

799 Samuel, J., Coulibaly, P., and Metcalfe, R.A.: Estimation of Continuous Streamflow in Ontario
800 Ungauged Basins: Comparison of Regionalization Methods, *J. Hydrol. Eng.*, 16, 447-459,
801 [http://dx.doi.org/10.1061/\(ASCE\)HE.1943-5584.0000338](http://dx.doi.org/10.1061/(ASCE)HE.1943-5584.0000338), 2011.

802 Sankarasubramanian, A., and Vogel, R.M.: Hydroclimatology of the continental United States,
803 *Geophys. Res. Lett.*, 30, 1-4, doi:10.1029/2002GL015937, 2003.

804 Santhi, C., Kannan, N., Arnold, J.G., and Diluzio, M.: Spatial calibration and temporal
805 validation of flow for regional scale hydrologic modeling, *J. Am. Water Resour. Assoc.*, 4, 829-
806 846, doi:10.1111/j.1752-1688.2008.00207.x, 2008.

807 Sawicz, K., Wagener, T., Sivapalan, M., Troch, P.A., and Carrillo, G.: Catchment classification:
808 empirical analysis of hydrologic similarity based on catchment function in the eastern USA,
809 *Hydrol. Earth Syst. Sc.*, 15, 2895-2911, doi:10.5194/hess-15-2895-2011, 2011.

810 Sefton, C.E.M., and Howarth, S.M.: Relationships between dynamic response characteristics
811 and physical descriptors of catchments in England and Wales, *J. Hydrol.*, 211, 11-16,
812 doi:10.1016/S0022-1694(98)00163-2, 1998.

813 Seibert, J.: Regionalization of parameters for a conceptual rainfall runoff model, *Agr. Forest*
814 *Meteorol.*, 98-99, 279-293, doi:10.1016/S0168-1923(99)00105-7, 1999.

815 Smakhtin, V.U.: Low flow hydrology: a review, *J. Hydrol.*, 240, 147-186, doi:10.1016/S0022-
816 1694(00)00340-1, 2001.

817 Tang, Y., Reed, P., Wagener, T., and van Werkhoven, T.: Comparing sensitivity analysis
818 methods to advance lumped watershed model identification and evaluation, *Hydrol. Earth Syst.*
819 *Sc.*, 11, 793-817, doi: 10.5194/hess-11-793-2007, 2007.

820 Tekleab, S., Uhlenbrook, S., Mohamed, Y., Savenije, H.H.G., Temesgen, M., and Wenninger, J.:
821 Water balance modeling of Upper Blue Nile catchments using a top-down approach, *Hydrol.*
822 *Earth Syst. Sci.*, 15, 2179-2193, doi:10.5194/hess-15-2179-2011, 2011.

823 Troch, P.A., Paniconi, C., and McLaughlin, D.: Catchment-scale hydrological modeling and
824 data assimilation, *Adv. Water Resour.*, 26, 131-135, doi:10.1016/S0309-1708(02)00087-8, 2003.

825 US Geological Survey: A National Water Information System, available at: <http://waterdata.usgs.gov/nwis/>
826 (last access 27 March 2014), 2014.

827 US Environmental Protection Agency and US Geological Survey: NHDPlus User guide,
828 available at: ftp://ftp.horizon-systems.com/NHDPlus/documentation/NHDPLUS_UserGuide.pdf
829 (last access November 2014), 2010.

830 van Griensven, A., Meixner, T., Grunwald, S., Bishop, T., Diluzio, and M., Srinivasan, R.: A
831 global sensitivity analysis tool for the parameters of multi-variable catchment models, *J. Hydrol.*,
832 324, 10-23, doi:10.1016/j.jhydrol.2005.09.008, 2006.

833 Vandewiele, G.L., and Elias, A.: Monthly water balance of ungaged catchments obtained by
834 geographical regionalization, *J. Hydrol.*, 170, 277-291, doi:10.1016/0022-1694(95)02681-E,
835 1995.

836 Viger, R., and Bock, A.: GIS Features of the Geospatial Fabric for National Hydrologic
837 Modeling, U.S. Geological Survey, Denver, CO, USA, doi:10.5066/F7542KMD, 2014.

838 Vogel, R.M.: Regional calibration of watershed models, *Watershed Models*, Singh, V.P., and
839 Frevert, D.F. (Eds.), CRC Press, Boca Raton, FL, USA, 2006.

840 Vrugt, J.A., ter Braak, C.J.F., Clark, M.P., Hyman, J.M., and Robinson, B.A.: Treatment of
841 input uncertainty in hydrologic modeling: Doing hydrology backwards with Markov Chain
842 Monte Carlo simulation, *Water Resour. Res.*, 44, W00B09, doi:10.1029/2007WR006720, 2008.

843 Wolock, D.M.: STATSGO soil characteristics for the conterminous United States. U.S.
844 Geological Survey Open-File Report 1997-656, Reston, VA, USA, available at:
845 <http://water.usgs.gov/GIS/metadata/usgswrd/XML/muid.xml>, (last access 3 March 2012), 1997.

846 Wolock, D.M., and McCabe, G.J.: Explaining spatial variability in mean annual runoff in the
847 conterminous United States, *Clim. Res.*, 11, 149-159, doi:10.3354/cr011149, 1999.

848 Zhang, X., Srinivasan, R., and Van Liew, M.: Multi-Site Calibration of the SWAT Model for
849 Hydrologic Modeling, *T. ASABE*, 51, 2039-2049, doi:10.13031/2013.25407, 2008.

850

851

852

853

854

855

856
857
858
859
860
861

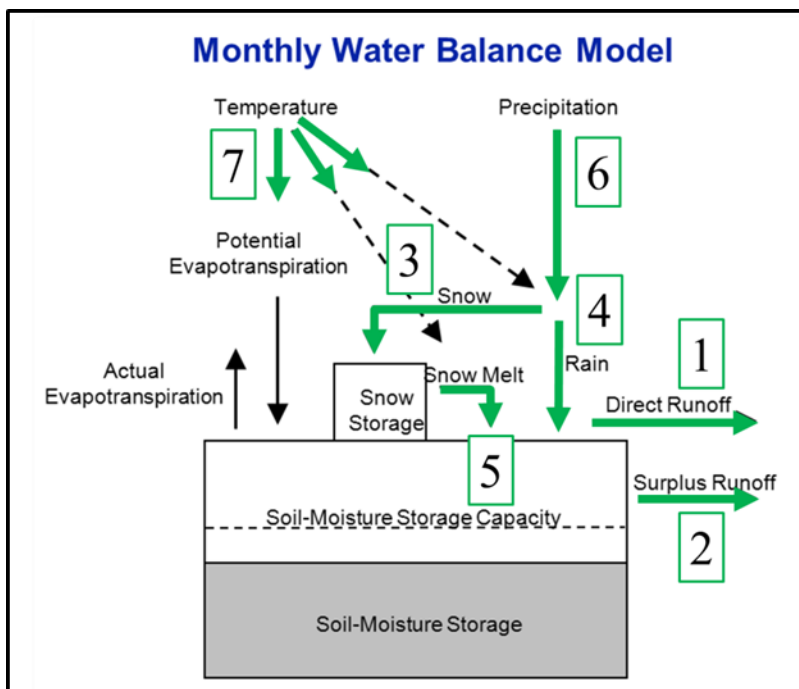
Parameter	Definition	Range	Default
1. <i>Drofac</i>	Controls fraction of precipitation that becomes runoff	0, 0.10	0.05
2. <i>Rfactor</i>	Controls fraction of surplus that becomes runoff	0.10, 1.0	0.5
3. <i>Tsnow</i>	Threshold above which all precipitation is rain ($^{\circ}\text{C}$)	-10.0, -2.0	-4.0
4. <i>Train</i>	Threshold below which all precipitation is snow ($^{\circ}\text{C}$)	0.0, 10.0	7.0
5. <i>Meltcoef</i>	Proportion of snowpack that becomes runoff	0.0, 1.0	0.47
6. <i>Ppt_adj</i>	Seasonal adjustment factor for precipitation (%)	0.5, 2.0	1
7. <i>Tav_adj</i>	Seasonal adjustment for temperature ($^{\circ}\text{C}$)	-3.0, 3.0	0

862
863
864
865
866

Table 1. Monthly Water Balance Model parameters and ranges.

867

868



869

870 Figure 1. Conceptual diagram of the Monthly Water Balance Model (McCabe and Markstrom
871 2007). Processes influenced by model parameters used in Fourier Amplitude Sensitivity Test
872 (FAST) those identified by green arrow and numbered 1-5 (Table 1).

873

874

875

876

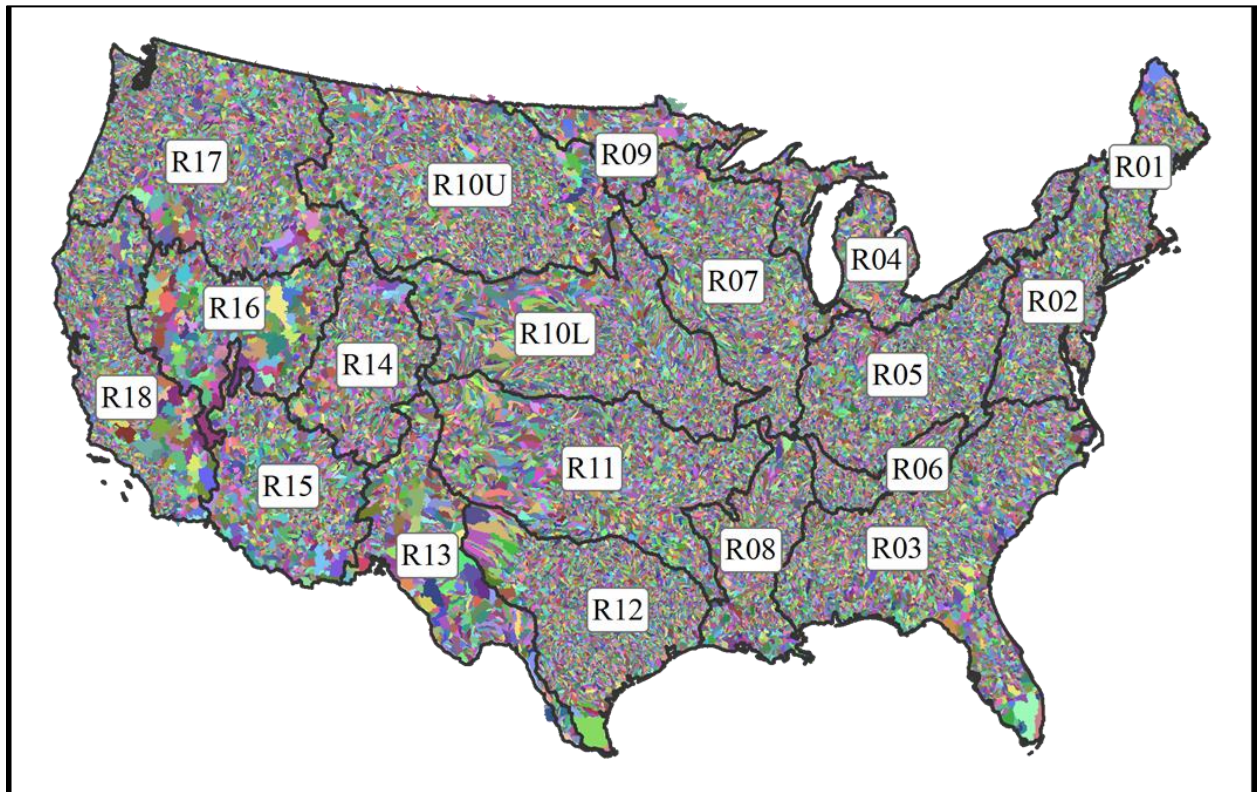
877

878

879

880

881



882

883 Figure 2. Hydrologic Response Units of the Geospatial Fabric, differentiated by color, overlain
884 by NHDPlus region boundaries (R01-R18).

885

886

887

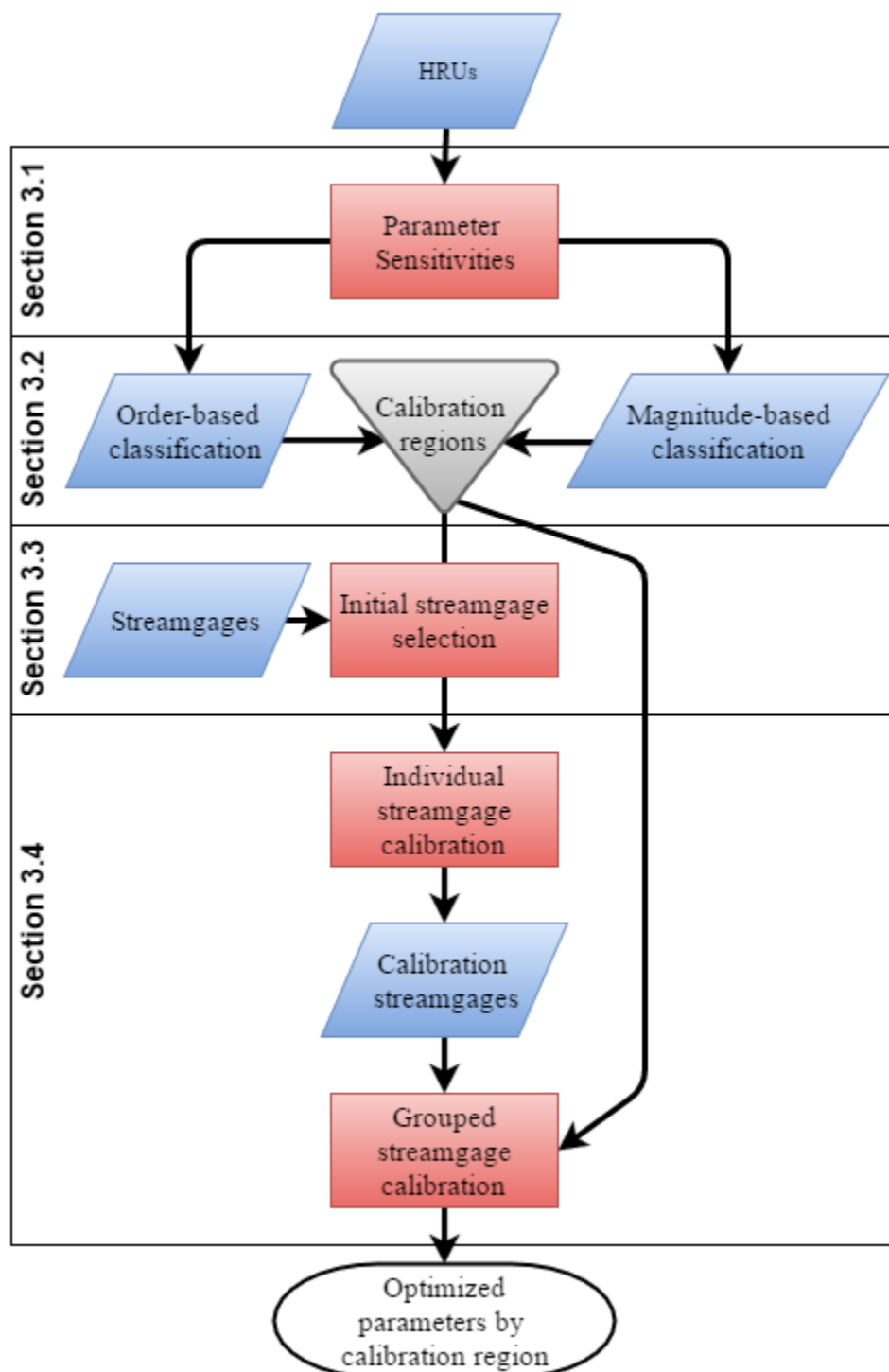
888

889

890

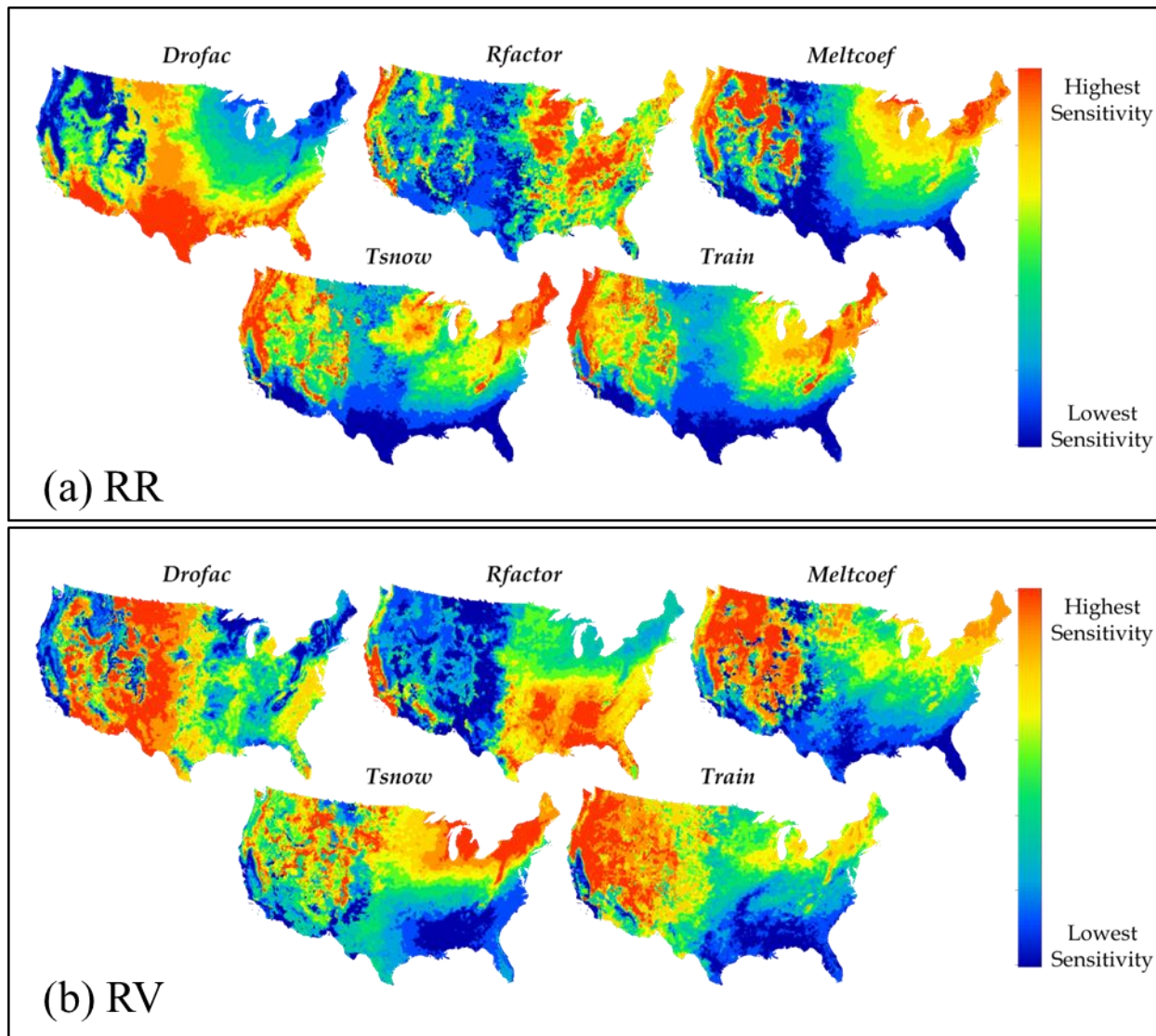
891

892



893

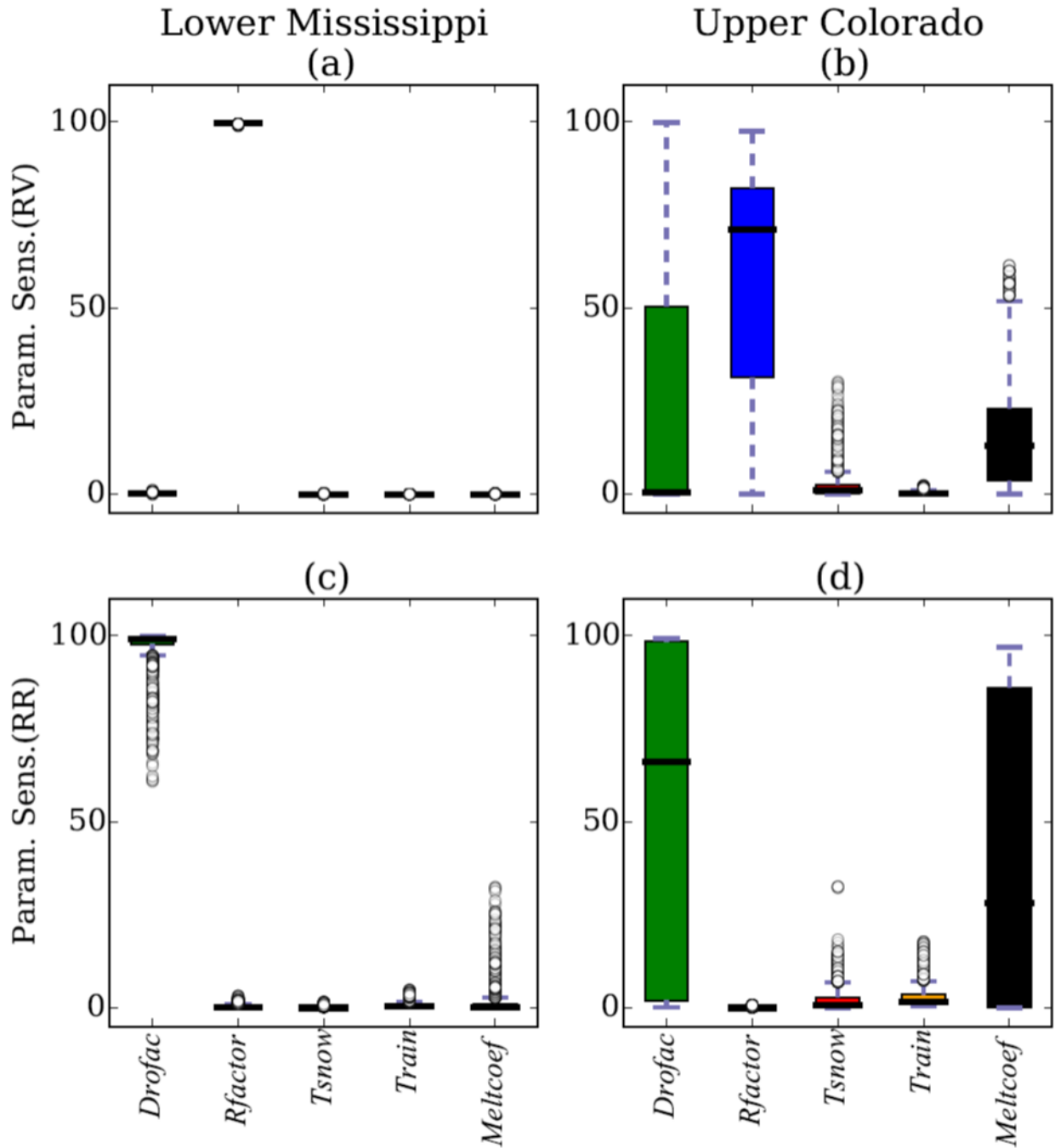
894 Figure 3. Schematic flowchart of the parameter regionalization procedure described in Section
895 3: Parameter sensitivities (3.1), Calibration regions (3.2), Initial streamgauge selection (3.3), and
896 Grouped streamgauge calibration (3.4).



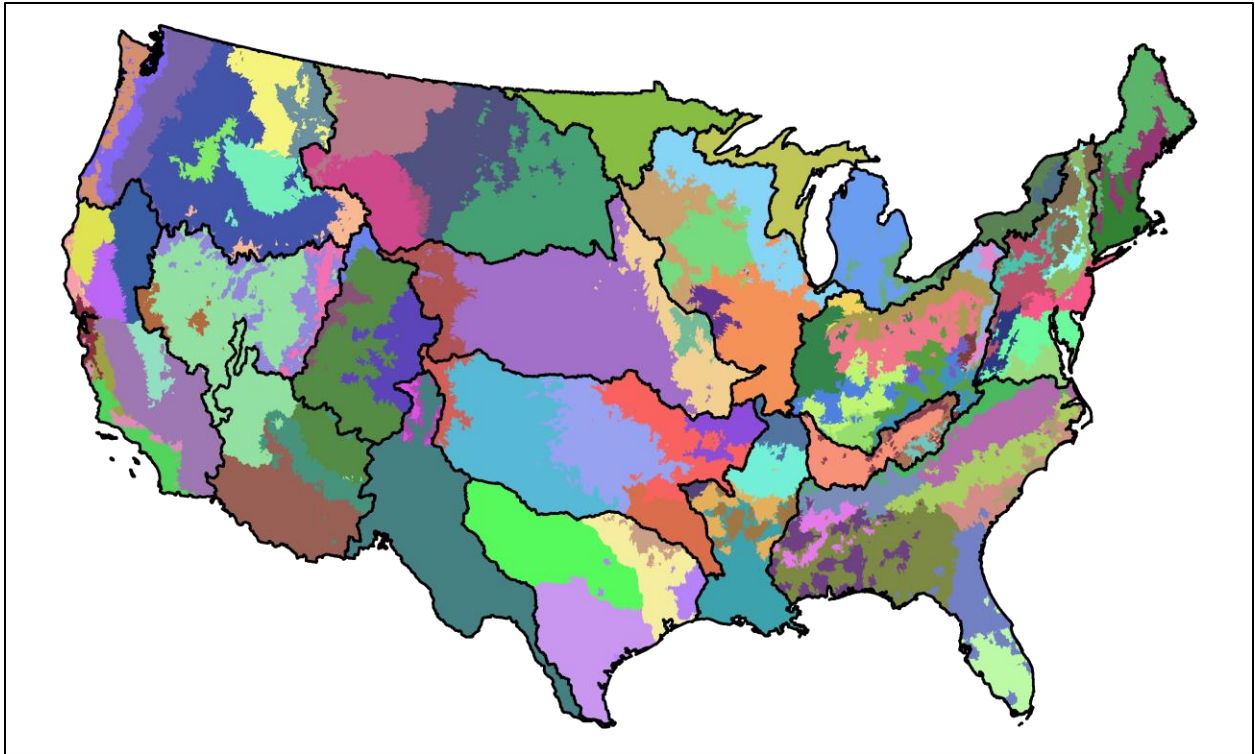
897
898 Figure 4. Relative sensitivity of the (a) Rainfall Ratio (RR) and (b) Runoff Variability (RV)
899 indices to Monthly Water Balance Model parameters.

900

901



903 Figure 5. Parameter sensitivities of Runoff Variability (RV; a and b) and Runoff Ratio (RR; c
 904 and d) indices for Monthly Water Balance Model parameters in the Lower Mississippi (R08) and
 905 Upper Colorado (R14).
 906



908

909 Figure 6. Final 110 Monthly Water Balance Model calibration regions differentiated by colors.
910 A subset of streamgages within each calibration region were calibrated in a group-wise fashion
911 to produce a single optimized parameter set for the entire region (Fig. 3).

912

913

914

915

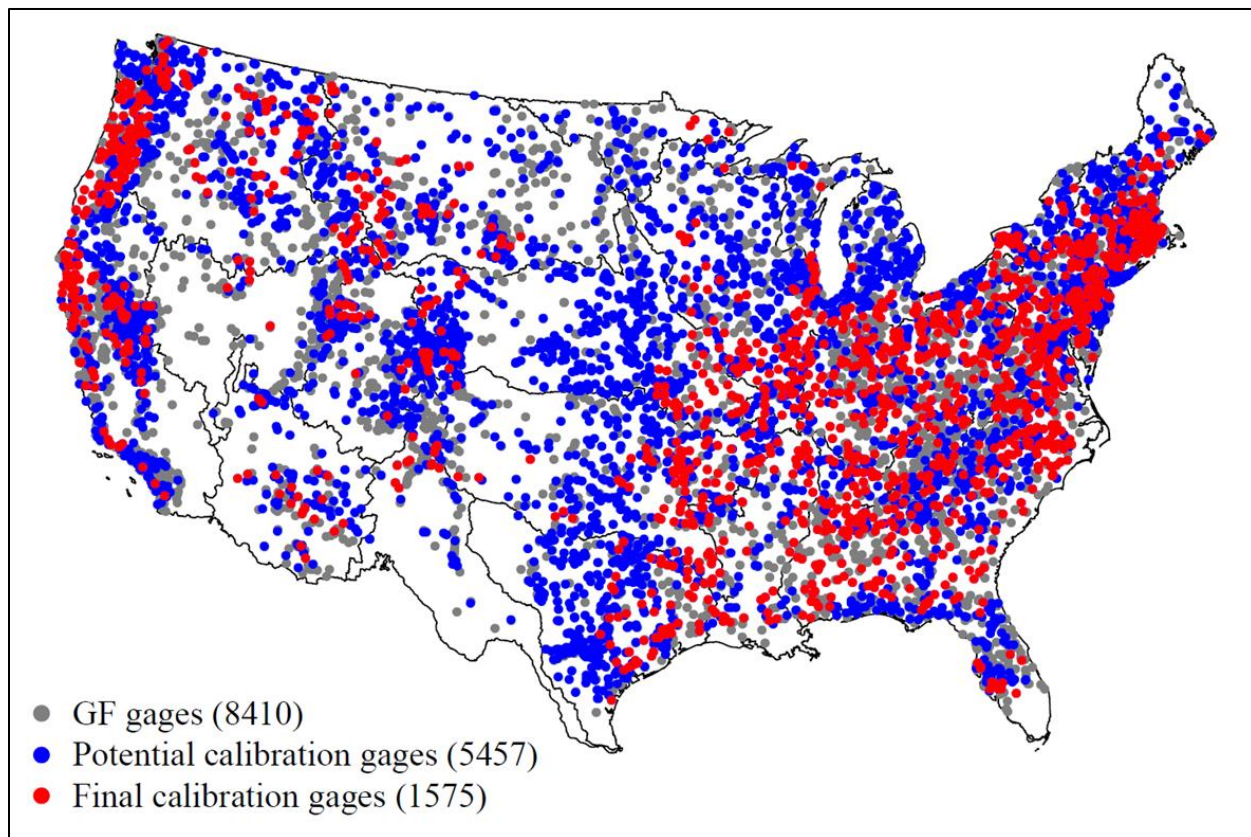
916

917

918

919

920



921

922 Figure 7. Streamgages tested in the study. GF notes geospatial fabric for national hydrologic
923 modeling (Viger and Bock, 2014).

924

925

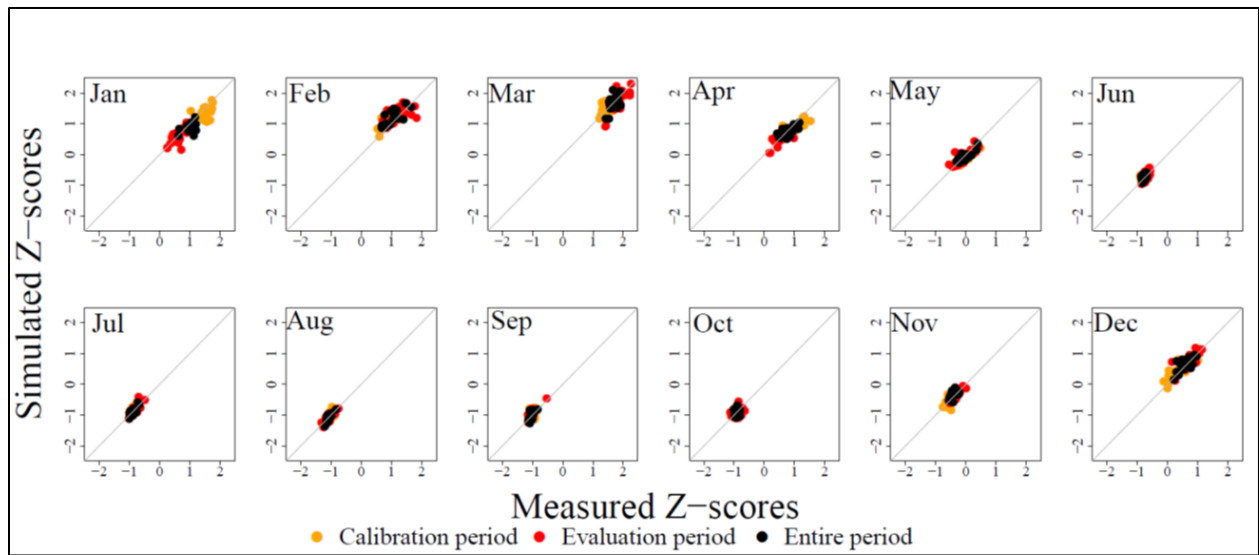
926

927

928

929

930



931

932 Figure 8. Measured versus simulated mean monthly Z-scores for the Tennessee River calibration
 933 region (see Fig. 9b for location). Orange is calibration, red is evaluation, and black is all years.

934

935

936

937

938

939

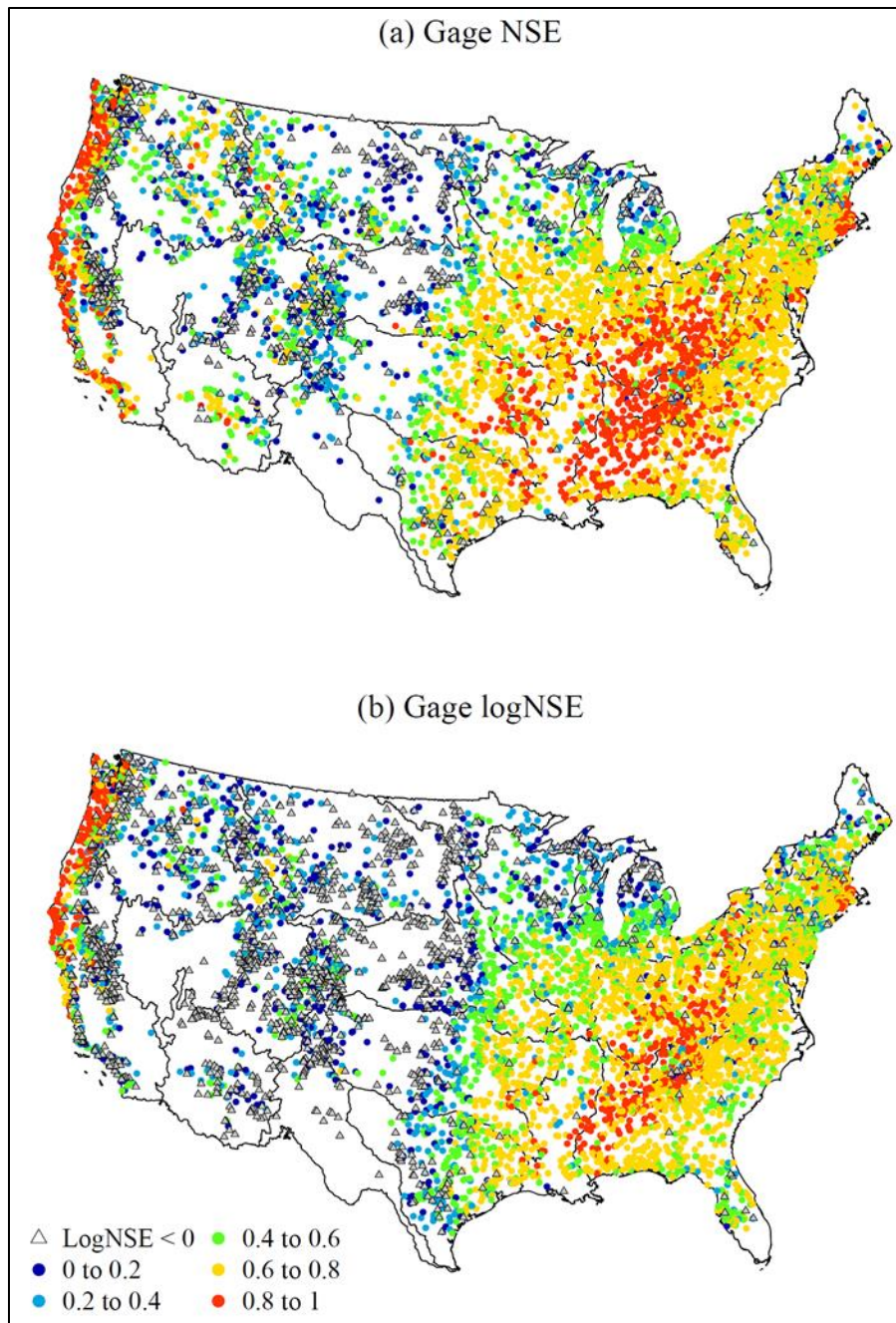
940

941

942

943

944



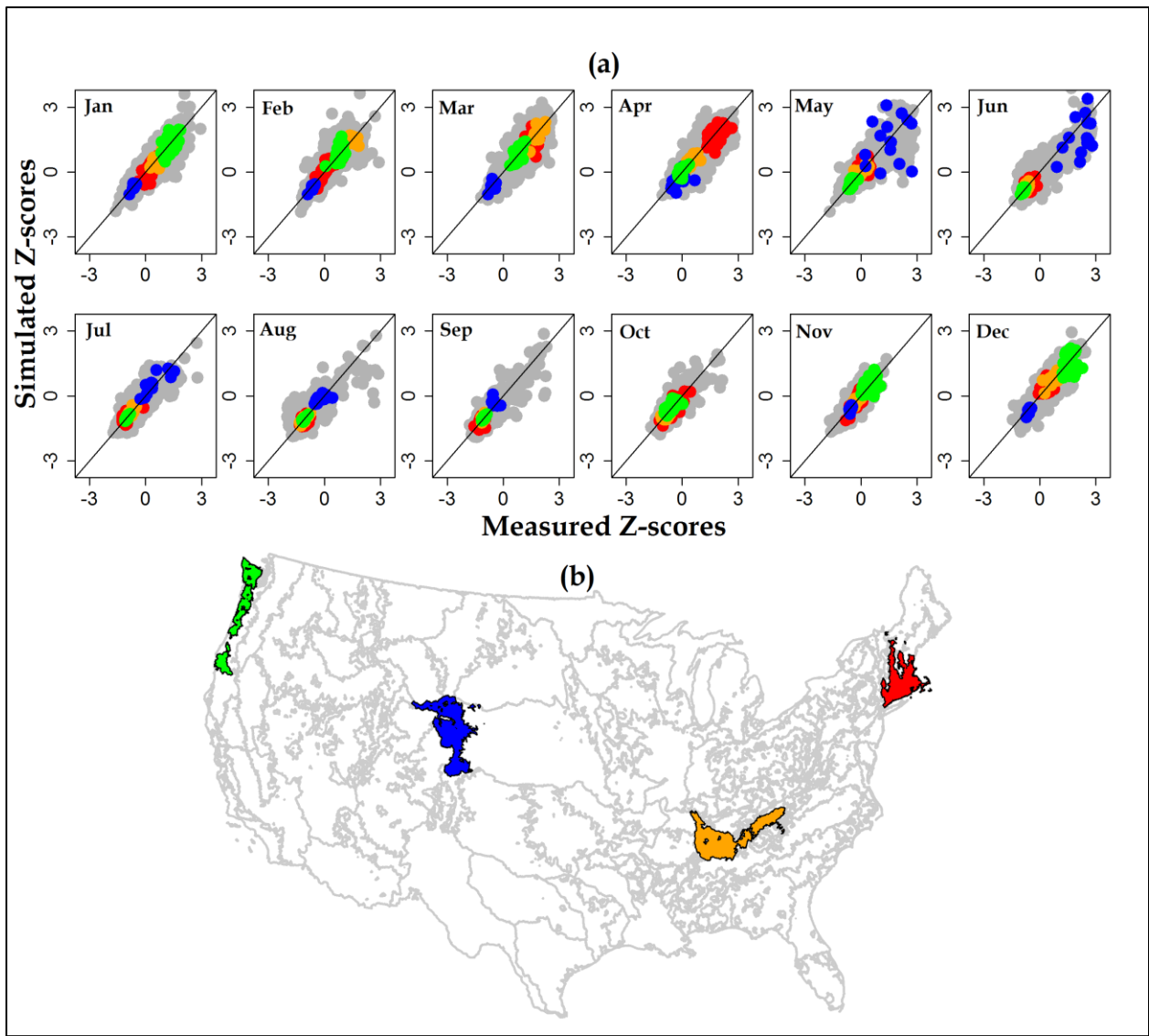
945

946 Figure 9. Individual streamgage calibration results: (a) Nash-Sutcliffe Efficiency (NSE)

947 coefficient and (b) log of the NSE (logNSE).

948

949



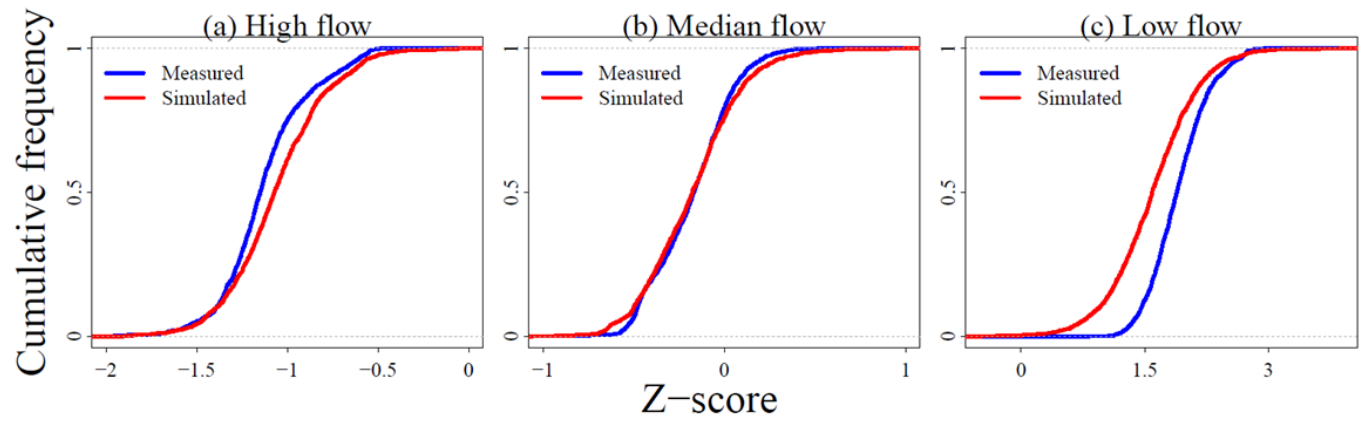
950

951 Figure 10. (a) Measured versus simulated mean monthly Z-scores for runoff at all streamgages
 952 and (b) location of highlighted streamgages for four calibration regions: New England (67
 953 streamgages, red); Tennessee River (21 streamgages, orange); Platte Headwaters (15
 954 streamgages, blue); and Pacific Northwest (33 streamgages, green).

955

956

957



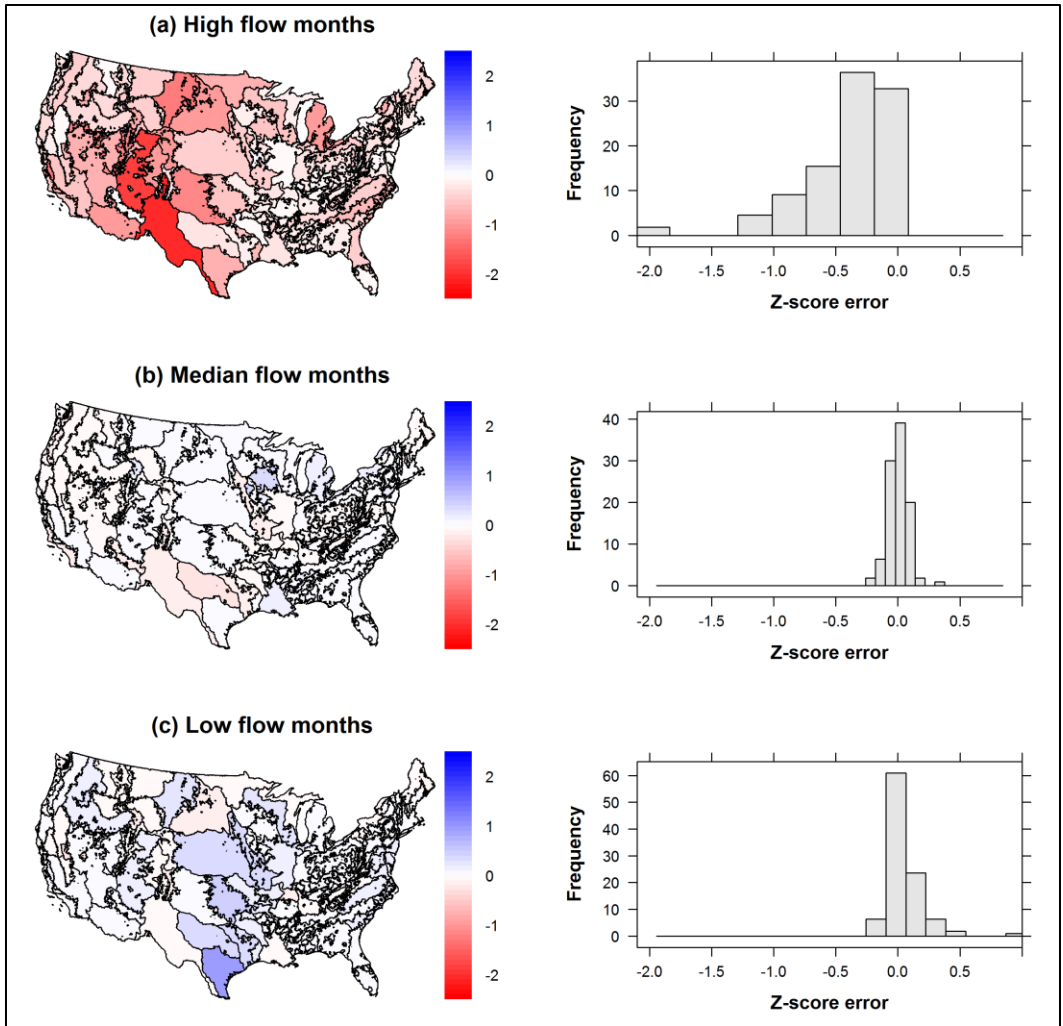
958

959 Figure 11. Z-score cumulative frequency for (a) highest-, (b) median-, and (c) lowest-flow

960

months.

961



962

963 Figure 12. Z-score error (simulated - measured) for (a) highest-, (b) median-, and (c) lowest-
 964 flow months.

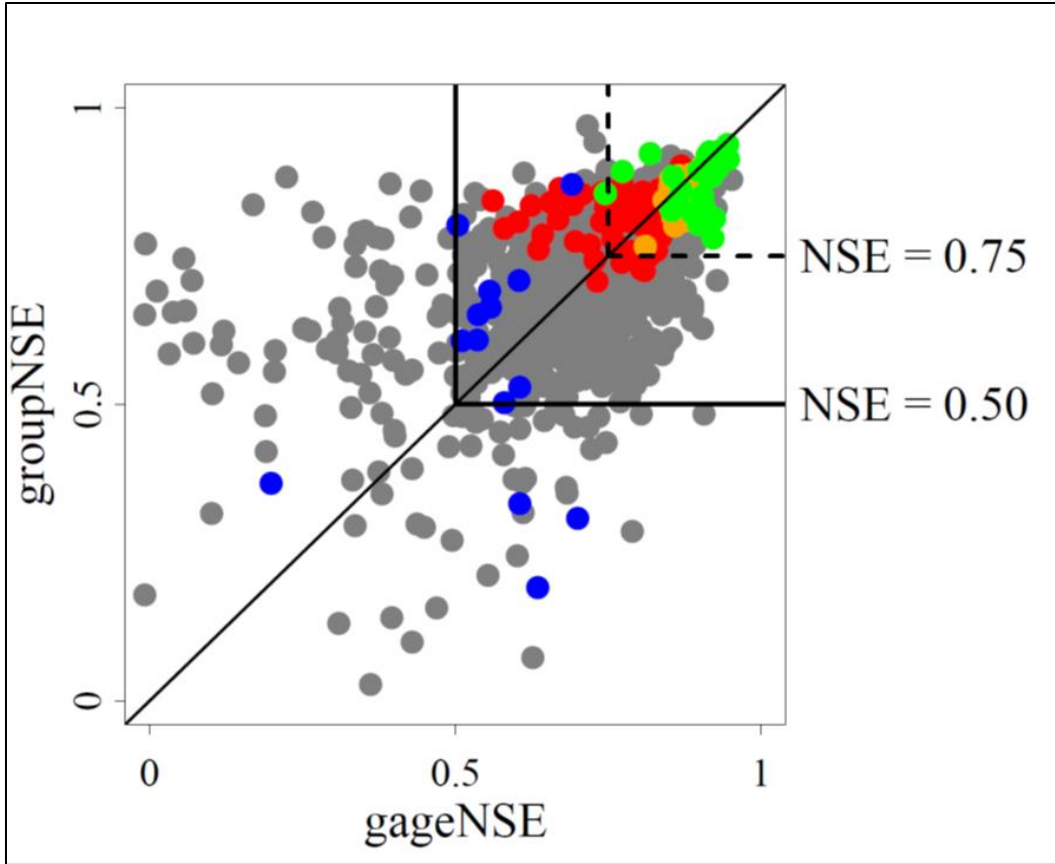
965

966

967

968

969



970

971 Figure 13. Nash Sutcliffe Efficiency from individual (gageNSE) and grouped (groupNSE)
 972 calibration. Calibration regions in New England (67 streamgages, red); Tennessee River (21
 973 streamgages, orange); Platte Headwaters (15 streamgages, blue); and Pacific Northwest (33
 974 streamgages, green) are highlighted (see Fig. 9b for location).

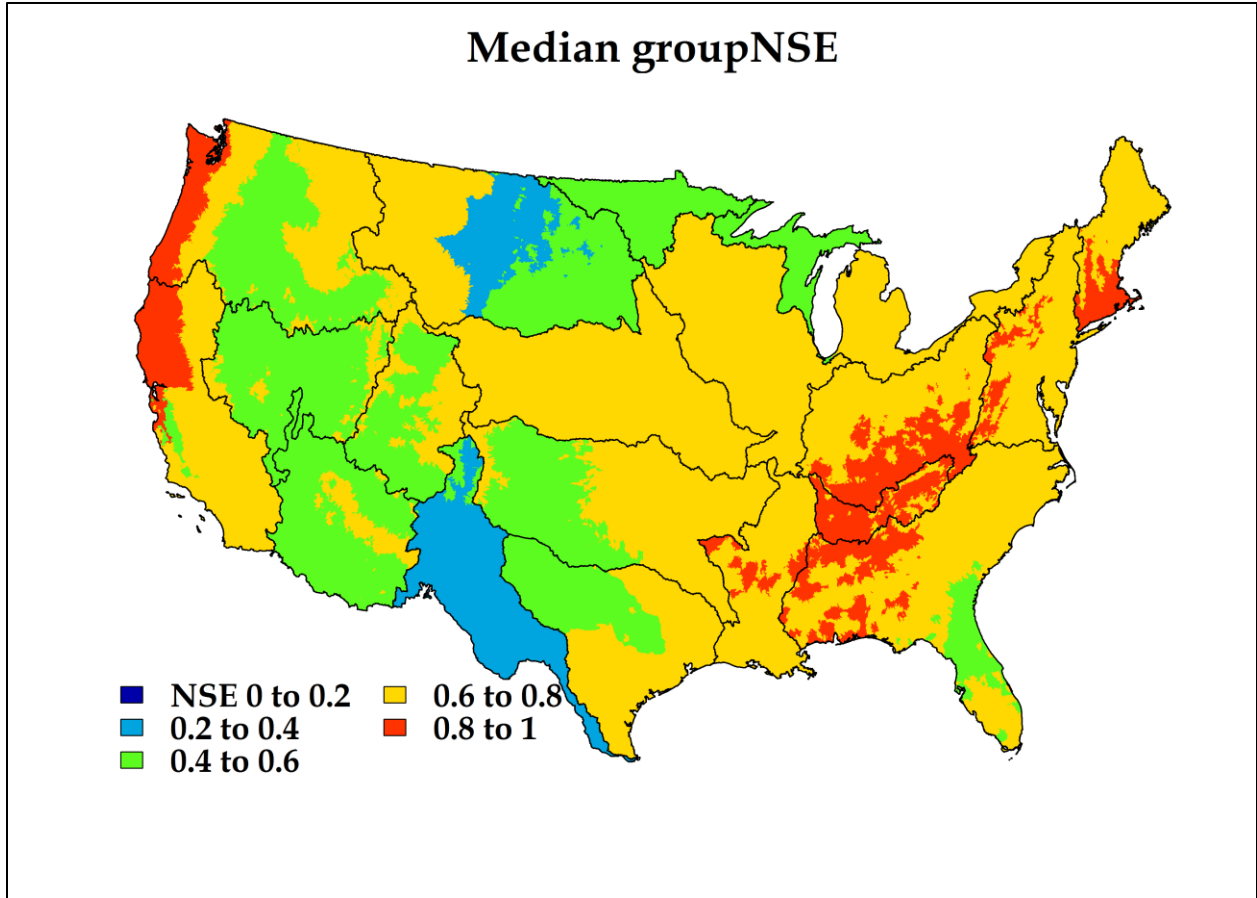
975

976

977

978

979



980

981 Figure 14. Median Nash Sutcliffe Efficiency (NSE) of streamgages used for calibration by
982 calibration region.

983

984